Separation & Purification Reviews
Publication details, including instructions for authors and subscription information:
http://www.informaworld.com/smpp/title~content=t713597294

Characterization of Crystallization Kinetics from Batch Experiments

Narayan S. Tavare

To cite this Article Tavare, Narayan S.(1993) 'Characterization of Crystallization Kinetics from Batch Experiments', Separation & Purification Reviews, 22: 2, 93 — 210
To link to this Article: DOI: 10.1080/15422119308544978
URL: http://dx.doi.org/10.1080/15422119308544978

SEPARATION AND PURIFICATION METHODS, 22(2), 93-210 (1993)

Review

CHARACTERIZATION OF CRYSTALLIZATION KINETICS FROM BATCH EXPERIMENTS

Narayan S. Tavare
Department of Chemical Engineering
University of Manchester Institute of Science and Technology
Manchester, M60 1QD England

ABSTRACT

This review outlines the techniques employed in experimental data reduction and analysis of batch crystallizers. A process description based on batch conservation equations describing population, mass and energy balances, both in crystal size and volume coordinate, together with appropriate kinetic events represented by phenomenological models and proper boundary conditions should be used in parameter identification. A number of general and useful techniques to extract growth and nucleation kinetics based on solution–side and solid–side information are reviewed. Procedures for parameter characterization for the phenomena of the growth rate dispersion and agglomeration are assessed.

CONTENTS

1. INTRODUCTION

1.1 Research Trend

Crystallization in the chemical industry is of enormous economic importance. Worldwide production rates of basic commodity products, such as sucrose,

salt, many fertilizers and other bulk chemicals all exceed 1 M t/annum and the demand is ever increasing. In the manufacture of these chemicals crystallization is an important step in a process sequence and an increased emphasis on the better integration of this step into the associated upstream and/or downstream processing operations is therefore needed. In addition as crystallization is a multidisciplinary subject interactions with bordering disciplines like physical chemistry, surface, material, mineral and biological sciences and chemical reaction engineering provide an important insight into the subject.

Industrial crystallization research associated with basic commodity products provided the initial impetus for continuous crystallizer studies in the early sixties. Fundamental research on the unit operation of crystallization was focused mainly on understanding and predicting the particulate nature of crystalline phase, recognizing that its better understanding and control would permit improvements of this unit operation, both as a separation and purification technique. The initial research work has proved the central importance of crystal size distribution in the design and performance of industrial crystallizers and provided as a unifying theme the interrelationships between the crystal size distribution on the one hand and crystallizer design criteria and operating problems on the other hand. Since then CSD studies have become a central part of industrial crystallization research.

In recent years the importance of fine chemicals and special effect high added value materials has increased in the competitive chemical industry. Consequently an increasing proportion of capital investment on research and development of such speciality products is being made at the expense of conventional large tonnage commodity products. Many speciality chemicals such as pharmaceuticals, agrochemicals, pigments, dyestuffs, catalyst, zeolites, proteins and food products involve crystallization or precipitation as crucial part of their manufacture and usually require batch processing because of their low tonnage capacity. High product purity and specific crystal size and habit may be desirable in many instances. Crystallization is also becoming increasingly important in many other rapidly expanding area such as biotechnology, mineral processing, waste treatment, pollution abatement, energy storage, new construction materials and electronic chemicals.

Batch crystallizers are extensively used in the chemical industry for the manufacture of many high added value fine chemicals. They are generally useful in small scale operation, especially when working with chemical systems which are difficult to handle due perhaps to their highly viscous or toxic properties. They are simple, flexible, require less investment and generally involve less process development. The purpose of this review is to summarize comprehensively our understanding of batch crystallization processes used in crystallization research for characterization of kinetic rates. In this paper a generalized analytical process description of a batch crystallizer, in both crystal size and volume coordinate, is developed and its applications will be illustrated to outline the techniques that are available to characterize crystallization kinetic processes including agglomeration and growth rate dispersion characteristics from batch crystallizer configurations. Crystallization can be approached from several points of view. This review primarily confronts solution crystallization. Over the past three decades enormous advances in the adoption of chemical engineering approaches to crystallization systems have paved the way in process identification analysis of crystallization configurations.

1.2 Batch Operation

The basic steps in a crystallization process are achievement of supersaturation, formation of crystal nuclei i.e. nucleation and their subsequent growth to form large crystals. All these three processes may occur simultaneously in a batch crystallizer. For the purpose of analysis crystallization in any configuration may be considered as a competitive process from the solution–side although as a consecutive process from the solid–side. Achievement of supersaturation may occur by cooling, evaporation, addition of precipitant or diluent, or by chemical reaction. Supersaturation in batch crystallization is usually generated by any one or a combination, in series or parallel, of these four main methods. For analysis it may be assumed that only one mode is dominant and the operation may be characterized by the mode. In general the corresponding analysis among different modes is, however, more or less similar and may be generalized. In cooling crystallizers supersaturation is generated because of the reduction in solubility with temperature; the solvent capacity of the

system remains approximately constant. In evaporative crystallizers supersaturation is produced by loss of solvent with subsequent reduction of solvent capacity with time; the solubility of a salt in solvent remains almost constant as the operation may be assumed isothermal. In dilution crystallizer generation of supersaturation is effected by the added diluent reducing the solute solubility and the solvent capacity of the system consequently increases with time. In reactive crystallizers supersaturation is created as a consequence of the production of a desired component by virtue of chemical reaction, solubility and solvent capacity may remain constant and both reaction and crystallization steps may be treated as occurring in series. Less conventional techniques of supersaturation generation by reverse osmosis and extreme pressure changes have been used. In reverse osmosis one of the ionic species is selectively transported through the membrane to generate the desired supersaturation while the solubility changes with the extreme pressure changes produce supersaturation, thus creating substantial driving force for solid deposition. Table 1 summarizes the techniques most commonly employed for supersaturation generation in systems crystallizing from solutions.

The proper mode, i.e. the technique employed to generate the supersaturation from a solution, is decided by the analysis of the system characteristics, yield and economic considerations in each mode of operation. Certainly there is a degree of flexibility in each mode of operation in order to control the performance of crystallizer. Usually a uniformity of critical rate or variable or optimality with respect to desired objective function can be considered. Table 2 provides a compilation of types of operation that have been reported for batch crystallizers in the literature!

1.3 Crystallization and Precipitation

There appears no clear distinction between crystallization and precipitation processes and the terms may be used interchangeably. The term '*crystallization*' is the more general description and can be thought of as encompassing the term '*precipitation*'. The latter is difficult to define precisely but it is generally used to describe the rapid crystallization of

Table 1: Techniques commonly used for supersaturation generation

mode	supersaturation produced by	solubility variation	examples
cooling	reduction in temperature	large with temperature	potassium nitrate, ammonium nitrate, sucrose
evaporation	loss of solvent	small with temperature	sodium chloride, ammonium sulphate, terephthalic acid,
vacuum	cooling, flashing evaporation	moderate with temperature	ammonium sulphate sodium sulphate, potassium chloride, Adipic acid
dilution	adding diluent	large with diluent concentration	proteins, dyes, pharmaceuticals, fine chemicals
reaction	generation of solute	may remain constant	ammonium sulphate, sodium perborate, calcium sulphate, speciality chemicals, multiphase systems

sparingly soluble materials usually as a result of an irreversible chemical reaction or physical change in the solution. Under such conditions relative supersaturation is comparatively high, so resulting in processes in which high nucleation rates prevail and crystal size is small. Further a precipitate

Table 2: Types of batch operation studied in each mode

mode	operating type
cooling	natural cooling
	constant cooling rate
	controlled to constant supersaturation
	controlled to constant supersaturation within metastable region
	size optimal control
evaporation	constant evaporation rate
	controlled to constant supersaturation
	controlled to constant supersaturation within metastable region
	optimal control
dilution	constant diluent addition rate
	constant rate of diluent concentration change
	controlled to constant supersaturation
	controlled to constant supersaturation within metastable region
	optimal control
reaction	various homogeneous and heterogeneous

frequently has a poorly–defined morphology. The possibilities of controlling such processes to achieve the desired product specifications are often limited due to the interplay between rapid kinetic events and external process conditions. Some of these generally valid points are highlighted in Table 3.

Table 3: Crystallization and Precipitation Processes

Description	Crystallization	Precipitation
Definition	in general solid phase formation	rapid crystallization
Solubility	wide range, usually medium to high	sparingly soluble
Generation of supersaturation	all possible modes	reaction and dilution
Relative supersaturation	low	high
Product morphology	well–defined	ill–defined
Product crystal size	large	small
Nucleation mechanism	secondary	primary
Nucleation rate	low	high
Nucleation order	low	high
Growth rate	wide range 0.005–0.5μm/s	low 0.005–0.05μm/s
Controllability	controllable	difficult to control

2. METASTABLE ZONE WIDTH

2.1 Solution Stability

The concept of supersaturation and the existence of the so–called metastable zone are useful in understanding the behaviour of the crystallizing system. Ostwald[2] first introduced the terms '*labile*' (unstable) and '*metastable*' supersaturation, referring to supersaturated solutions in which spontaneous deposition of solid phase, in the absence of solid nuclei, will or will not occur, respectively. On the basis of extensive research into the relationship between supersaturation and spontaneous crystallization Miers pointed out that there exists supersolubility curve for every solute–solvent system which is almost

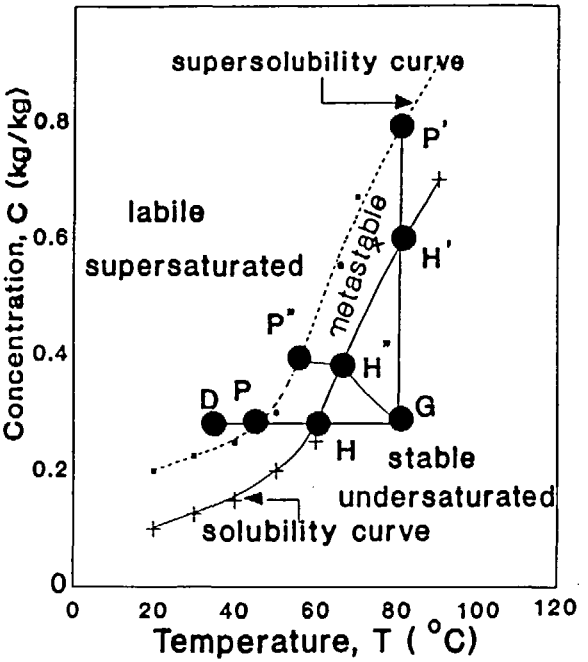

Figure 1 Miers plot for a typical salt

parallel to the solubility curve as depicted in Miers plot for a typical salt (Figure 1). The lower solid continuous line is the normal solubility curve for the salt concerned. The upper broken curve, generally referred to as supersolubility curve, represents temperatures and concentrations at which spontaneous crystallization occurs. As the spontaneous crystallization point depends on many variables the supersolubility curve is not so well defined as the solubility curve and may be visualized as a narrow band located in the supersaturation zone. Despite its ill–definition it is generally accepted that a region of metastability exists above the solubility curve in the supersaturated region. The Miers plot is divided into three zones:

1. The well–defined stable (undersaturated) zone where crystallization is not possible.

2. The variable metastable (supersaturated) zone between the solubility and supersolubility curves where spontaneous crystallization is not possible.
3. The unstable or labile (supersaturated) zone where spontaneous crystallization is possible, but not inevitable.

The path followed in a crystallization process can be mapped in the concentration–temperature plane as in the Miers plot. If a solution represented by point G in Figure 1 is cooled without loss of solvent (line GHP) spontaneous crystallization cannot occur until conditions represented by point P are reached. At this point the first indication of crystallization, either spontaneous from solution or induced by seeding, agitation or mechanical shock, will appear and further cooling to some point D for some salts may be necessary before crystallization can be induced. Supersaturation can also be achieved by evaporating some of the solvent from solution. Vertical line GH'P' in Figure 1 represents such an evaporation operation carried out at constant temperature. Penetration beyond the supersolubility curve may rarely occur as the bulk of the solution is usually supersaturated to a lesser degree than the surface from which evaporation takes place. A combination of cooling and evaporation as shown by curve GH"P" in Figure 1 may be employed in actual practice as in vacuum cooling.

2.2 Experimental Determination

Many studies, mainly employing cooling crystallization mode, have been reported on the measurement of metastable zone width in the literature (see for example Table 1 in Tavare[1]). Two distinct experimental techniques have been used in their determination. In the first technique a solution of known saturation temperature is cooled at a constant rate to a critical temperature at which the onset of nucleation or changes in solution physical state are detected. The difference between the critical and saturation temperatures gives the maximum allowable undercooling for the cooling rate used. Both temperature and supersaturation vary with time. In the second technique the induction period, i.e. the time elapsed between the achievement of

supersaturation and the onset of nucleation detected either by solid appearance or change in some suitable solution physical property, is determined as a function of supersaturation. Both temperature and supersaturation remain constant during the experiment until the onset of nucleation since the achievement of the initial supersaturation can generally be accomplished quickly. The supersaturation corresponding to chosen critical induction time may be used as a metastable zone boundary.

The metastable zone width depends not only on many factors including temperature, cooling or evaporation rate (i.e., supersaturation generation rate), agitation, thermal history, presence of seeds and impurities etc. but also on the method of detection. The normally accepted metastable limit defined as the temperature at which the given solution nucleates spontaneously and measured in the laboratory under carefully controlled conditions is useful for giving some indication of the relative stability of supersaturation and may provide a guideline in choosing the actual working level of supersaturation in the crystallizer configuration. The most important requirement however is that it must be determined in the presence of the crystalline phase and the actual mother liquor to be processed. The use of experimentally measured metastable zone width in characterization of nucleation kinetics will be discussed later in the section on parameter characterization of nucleation process.

3. CRYSTALLIZATION KINETICS

The essence of effective characterization of crystallization kinetics and their successful application in crystallizer design and analysis resides in the recognition that all the kinetic events are rate processes. Although several kinetic events are identifiable in a crystallizer operation crystallization kinetics in the literature are conventionally characterized in terms of two dominant rate processes, viz. crystal growth and nucleation. Both the term '*rate*' and its concept need careful definitions. At the outset it is necessary to emphasize the distinction between *process rate* and *rate of change* while establishing kinetic

correlations as has been suggested in the analysis of multiphase reactor systems.[3,4] The rate of change follows the dictionary definition as familiar from the calculus, has derivative character and is subject to measurement. The process rate, as used in crystal nucleation or growth rate, is just a concept and always important in process analysis. One does not measure process rates directly, but only arrives at their values by some combination of measurement and theory.

Although a large fraction of efforts were directed towards developing rate models and analytical solutions for the rate processes, both by continuous (analytical) and discrete (numerical) mathematical methods the crystallization literature of engineering practice is still largely based on experimental data yielding empirical correlations. These correlating equations have been relatively uninfluenced by theory as most theoretical solutions in most cases provide no guidance for the functional behaviour. Most analytical solutions are subject to uncertainty arising primarily from simplification and idealization both in model formulation and evaluation. Uncertainty and imprecision in experimental data may arise not only from incomplete definition and control of experimental environment but also from errors of measurements. Empirical observations along with theoretical support provide a sound basis for correlating equations over wide range of variables.

3.1 Nucleation

Formation of new crystals may result from any one, or a combination, of different mechanisms (primary, homogeneous or heterogeneous and secondary nucleation) or by attrition. In an industrial crystallization practice secondary nucleation has a predominant influence as indicated by the informative experimental evidence.[5-7] The nucleation rate expressed as number per unit mass of solvent per unit time may in general be expressed by the semi–empirical equation

$$B = k_b \mu_k^j \Delta c^b \qquad (1)$$

The nucleation rate constant k_b may be a function of many other variables, in particular temperature, hydrodynamics, presence of impurities and perhaps some crystal properties, and the effects of these might be incorporated in the rate equation using suitable functional forms. The power law term μ_j^k represents the kth moment of the crystal size distribution present in the crystallizer. Normally the use of the third moment, i. e. slurry concentration or magma density, is found suitable to account for secondary nucleation effects. Thus equation (1) with k = 3 can satisfactorily be used to represent the nucleation rate as

$$B = k_b M_T^j \Delta c^b \tag{2}$$

in an industrial situation. A power law term of energy input per unit suspension volume, impeller speed or stirrer speed, representing a measure of the fluid mechanics effect on the secondary nucleation may be incorporated in equation (1). It is possible to specify the nucleation rate on different basis. Sometimes it is convenient to express the nucleation rate in terms of solute mass deposition per unit mass of solvent per unit time as

$$B_s = k_B M_T^j \Delta c^b \tag{3}$$

Typical values of b lie between ~ 0.5 and 2.5 for secondary nucleation rates and higher (up to 10 or so) for primary nucleation rates. In cases where the secondary nucleation is dominant most values of j are close to unity perhaps suggesting the dominance of collisions between crystals and stirrer or vessel walls rather than between two crystals; occasionally much lower values of j in secondary nucleation studies have been suggested (e. g. 0.4 for K_2SO_4[8]; 0.14 for KCl[9]). When primary nucleation mechanism is significant the influence of the particle concentration on the nucleation rate should be absent. The range of exponent of stirrer speed predicted by semi–theoretical secondary nucleation models based on contact mechanisms is from 2 to 4 and of that measured is from 0 to 8[6,7] Primary nucleation rates can also be increased by the mechanical energy inputs to the systems but may not be reduced by reduction in contact energy. Several studies[10-13] demonstrated significant

(~3–10 fold) reductions in nucleation rates just by replacing a stainless steel agitator with one from another soft material. It is most common practice to determine the kinetic parameters in any nucleation correlations from empirical observations employing established techniques.

3.2 Crystal Growth

Various theories have been evolved to represent the growth process taking place at different magnification levels spanning from atomic to macroscopic scale and to develop growth rate expressions theoretically. These attempts based on certain presumptions have not yet led to convenient working relationships for pragmatic situations. For engineering purposes in crystallizer design and assessment the simple empirical power law relationship expressing the specific rate of mass deposition per unit crystal surface area by

$$R \equiv \frac{1}{A_T}\frac{dW}{dt} = k_G \, \Delta c^g \tag{4}$$

is found to be most useful. The order, g, of the overall growth process is generally between 0 and 2.5, order around unity being the most common. In general, the overall rate constant, k_G, depends on temperature, crystal size, hydrodynamic situation and presence of impurities. The effect of the temperature on the overall growth rate constant may normally be expressed by an Arrhenius relation. Size dependence of the growth rate constant may be attributed to hydrodynamic environments surrounding the growing crystal or crystal surface or shape characteristics and may be expressed by one of several models. The simple power law term as in the case of the Bransom growth rate model may be an example of such models. The slurry voidage and intensity of agitation may influence the characteristic turbulence and the relative crystal solution velocity in the suspension. To account for the effect of slurry voidage and solid fraction on the overall growth rate constant a simple empirical power law term of the ratio of the slurry voidage to the solid fraction may be incorporated. A power law term for stirrer speed and an exponential term of

impurity concentration may also be included. Thus Palwe et al.[14] modified equation (4) to a general growth rate model as

$$R = aL^f \exp(-\frac{E_g}{R_g T}) (\frac{\epsilon}{1-\epsilon})^e N^m \exp(kI) \Delta c^g \quad (5)$$

The crystal growth rate in terms of mass deposition may be specified in terms per unit crystal weight (i. e., kg/kg s) in crystal suspension, especially in fluidized bed, rather than in per unit crystal surface area (i. e., kg/m^{2}s). Instead of mass deposition growth rate (equation (4 or 5)) it is convenient to express it as an overall linear growth rate as

$$G = k_g \Delta c^g \quad (6)$$

It is important to note that the overall linear growth rate (used as process rate) is specific with respect to crystal number as the mass deposition growth rate is with respect to surface area. The consistent definition of the linear growth rate in a multiparticulate batch system where the total number of crystals is changing in the ensemble is time rate of change of total length of all crystals per crystal and not the time rate of change of a crystal size.

4. PROCESS REPRESENTATION

The purpose of this section is to represent the basic process configuration which may be useful in assessing the several techniques available for the process identification and modes of crystallizer operations with appropriate modifications. Usually two types of information can be made available from a seeded isothermal operation, the solution–side information representing the supersaturation–time variation, i.e. the desupersaturation curve, and the solid–side information depicting the population density as a function of time and size. If only the solution–side information is available then the two processes viz crystal nucleation and growth are generally assumed competitive. The nucleation rate is expressed in terms of solute mass deposition rate per unit mass of solvent while the growth rate is the solute deposition rate per

unit surface area. In many cases nucleation rate may be assumed negligible. The process based only on the solution–side information will be described in the next section.

4.1 Solution–side Information

For a constant volume isothermal batch crystallizer a supersaturation balance can be written as

$$-\frac{d\Delta c}{dt} = B_s + A_T R = k_B M_T^j \Delta c^b + k_G A_T \Delta c^g \tag{7}$$

In equation (7) nucleation rate defines the specific rate of solute deposition in the nucleation process while the product of specific mass deposition rate and specific crystal surface area represents that of the growth process. Assuming constant crystal shape factors and negligible breakage and agglomeration the magma density, crystal surface area, average size and slurry voidage are defined as

$$M_T = M_{T0}(W/W_0) \tag{8}$$

$$A_T = A_{T0}(W/W_0)^{\frac{2}{3}} \tag{9}$$

$$\bar{L} = \bar{L}_0(W/W_0)^{\frac{1}{3}} \tag{10}$$

$$\epsilon = 1 - (W/\rho_c V) \tag{11}$$

where

$$W = W_0 + (\Delta c_0 - \Delta c)S \tag{12}$$

The initial values M_{T0} and A_{T0} can be evaluated from the initial weight and size of seed crystals through the expressions

$$A_{T^0} = FW_0/(\rho_c \bar{L}_0 S) \tag{13}$$

and

$$M_{T^0} = W_0/S \tag{14}$$

The desupersaturation curve (Δc–t) for a given set of parameters can be generated numerically by integrating the supersaturation balance equation (equation 7). Typical desupersaturation curve and its rate curve ($\Delta \dot{c}$–t) calculated for parameters in Table 4 using the fourth order Runge Kutta with an integration step length of 30 s is shown in Figures 2 and 3, respectively. The smooth solid curves are drawn using the actual numerical values obtained from the supersaturation balance equation (equation 7) using the assumed known kinetic parameters. The simulated data points were taken from these solid curves at suitable time intervals representing the results of experimental measurements. In these case thirty data points were chosen; the time interval between these points being initially 30s, increasing to 510s at the end of the batch time. The calculated data points represent the derived from the supersaturation balance equation (equation 7) using the estimated kinetic parameters. The desupersaturation curve decays continuously but its rate usually passes through a maximum in an isothermal seeded batch crystallizer initially charged with supersaturated solution. The relative magnitude of the growth and nucleation terms in the supersaturation balance equation (equation 7) as defined by the ratio of the mass deposition rate by growth to that by nucleation is important in influencing the nature of desupersaturation and desupersaturation rate curves and its variation is included in Figure 3. Depending on the process and kinetic parameters the overall operation may range from no to very rapid desupersaturation, total to negligible domination of nucleation or growth process over a part of or whole period of the process.

4.2 Solid–side Information

In the solution–side representation continuity of the supersaturation was tacitly assumed. During an isothermal batch operation a seeded crystallizer will however contain two types of crystals and so the general solution to the

Table 4: Parameters used in calculation of the batch response (Figures 2–5)

Batch time, τ(s)	5400
Solubility, c*(kg solute/kg solvent)	0.1243
Initial supersaturation, Δc_0(kg /kg solvent)	0.015
Seed size, $\bar{L}_0(\mu m)$	550
Crystal density, ρ_c(kg/m^3)	2660
Solvent capacity, S(kg water)	25.46
Specific seed loading, W_0/S (kg /kg solvent)	3.9×10^{-4}
Volume shape factor, k_v	0.525
Ratio of surface to volume shape factor, F	7.0
For solution–side information (desupersaturation curve)	
Growth rate order,g	2.0
Growth rate coefficient, k_G(kg/m^{2}s(kg/kg)^2)	1.0
Nucleation order, b	4
Nucleation rate coefficient, k_B (kg/kgs(kg/kg)$^{b+1}$)	5×10^4
Exponent of magma density, j	1.0
For solid–side information (population density curves)	
Growth rate order, g	1.5
Growth rate constant, k_g(m/[s (kg/kg)^g])	$5.x10^{-5}$
Nucleation order, b	3.0
Exponent of magma density, j	1.0
Nucleation rate constant, k_b (no/[kg s (kg/kg)$^{b+j}$])	1×10^{11}
Relative nucleation to growth order, i	2.0
Relative nucleation rate constant, K_R (no/[kg s (kg/kg)^j(m/s)^i])	4×10^{19}
Number of grids	500
Maximum size for N crystals(μm)	1000

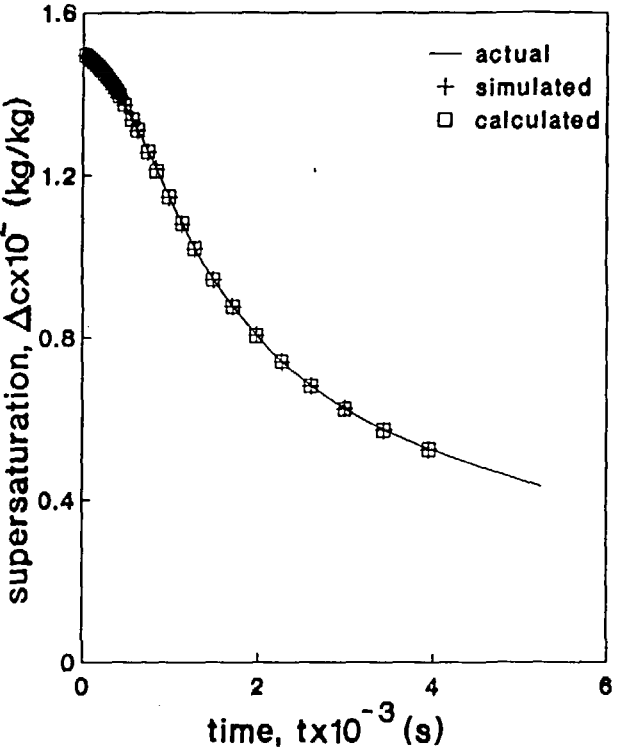

Figure 2 Typical desupersaturation curve (data in Table 4)

population balance equation should comprise one part representing the population density of the seeds and the other that of nuclei subsequently generated. It is convenient to use the convention suggested by Jones and Mullin[15] and distinguish between the seed crystals as S crystals and the nuclei as N crystals; their respective number densities being continuous functions of size and time. As the working solvent capacity of a batch crystallizer may be time varying it is convenient to define the population density function, n, based on the total solvent capacity at any time as

$$\hat{n} = nS \tag{15}$$

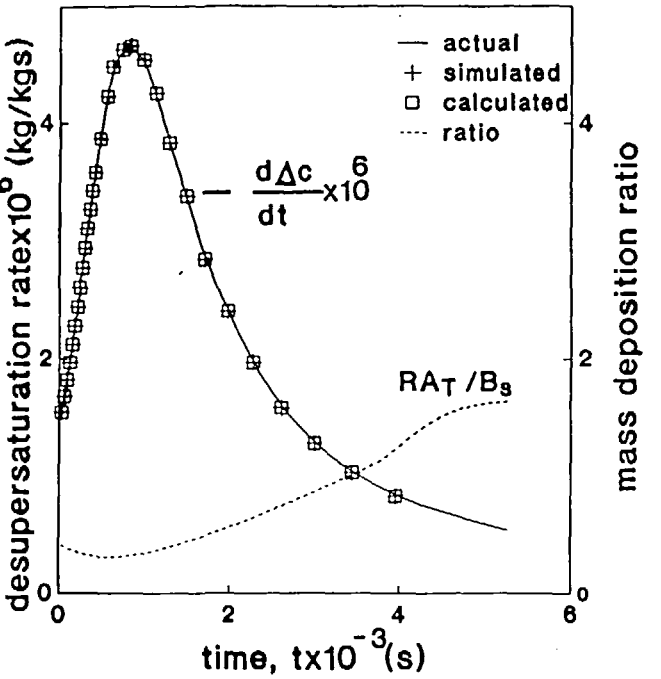

Figure 3 Desupersaturation rate curve (data in Table 4 and Figure 2)

For a perfectly mixed batch crystallizer in which crystal breakage and agglomeration are negligible the population balance equation for size independent growth rate is[16]

$$\frac{\partial \hat{n}}{\partial t} + G \frac{\partial \hat{n}}{\partial L} = 0 \tag{16}$$

where $\hat{n}$ is the population density based on total solvent capacity at any time and G is the overall linear growth rate.

The boundary condition for the nuclei population density can be represented by the relation

$$\hat{n}(t,0) = \hat{n}^0 = \frac{\hat{B}}{G} = K_R M_T^j G^{i-1} \tag{17}$$

where i is the relative kinetic order (= b/g) and K_R is the relative nucleation rate constant (= k_b/k_g^i). $\hat{B}$ represents the total nucleation rate defined in terms of flux added at crystal size very close to zero in the batch at any time t. The moment equations for N crystals obtained by moment transformation of the population balance equation (equation 16) with respect to size are

$$\frac{d\hat{\mu}_0}{dt} = \hat{B} \tag{18}$$

$$\frac{d\hat{\mu}_1}{dt} = \hat{\mu}_0 G \tag{19}$$

$$\frac{d\hat{\mu}_2}{dt} = 2\hat{\mu}_1 G \tag{20}$$

$$\frac{d\hat{\mu}_3}{dt} = 3\hat{\mu}_2 G \tag{21}$$

In a batch crystallizer the rate of solid deposition based on the total solvent capacity at any time on the S crystals alone is

$$\frac{d\hat{W}_S}{dt} = \frac{3\hat{W}_0 L_S^2 G}{\bar{L}_0^3} \tag{22}$$

while that for the N crystals will be

$$\frac{d\hat{W}_N}{dt} = k_v \rho_c \frac{d\hat{\mu}_3}{dt} = \frac{3k_v\rho_c}{k_a} \hat{A}_N G \tag{23}$$

The supersaturation balance for this configuration can therefore be written as

$$-\frac{d\hat{\Delta}c}{dt} = \frac{d\hat{W}_S}{dt} + \frac{d\hat{W}_N}{dt} = \frac{3\hat{W}_0 L_S^2 G}{\bar{L}_0^3} + \frac{3\rho_c k_v \hat{A}_N G}{k_a} \tag{24}$$

The solute mass balance for this configuration in terms of the total mass deposition of the solute can be expressed as

$$\frac{d\hat{c}}{dt} + \frac{d\hat{W}}{dt} = 0 \tag{25}$$

The variation of the largest nuclei size starting from L = 0 at t = 0 can be represented as

$$\frac{dL}{dt} = G \tag{26}$$

The population balance equation coupled with the supersaturation or mass balance equation through the set of moment equations represents mathematically the batch crystallizer configuration generally used in determination of crystallization performance characteristics.

For a non–isothermal batch crystallizer operation the additional balance equation needs to be considered. In the case of a cooling crystallizer the heat needs to be removed from the system while it is supplied at a desired rate to evaporate the solvent in an evaporative crystallizer as a process requirement. In some cases there may be additional energy requirement due to process heat sinks or sources released as heat of crystallization and/or heat of reaction. Generally simple expressions for solubility variation with temperature, rates for cooling, evaporation or dilution are used for analysis in a given mode of operation. For real systems operated in a batch crystallizer complex relations and combinations of different modes in series and/or parallel may be encountered.

4.3 The Batch Population Density Function

To determine the batch population density as a function of time and size the population balance equation describing the batch crystallizer (e.g. equation 16) must be solved under the constraints of batch operation. A number of solution techniques are available and some of the important analytical and

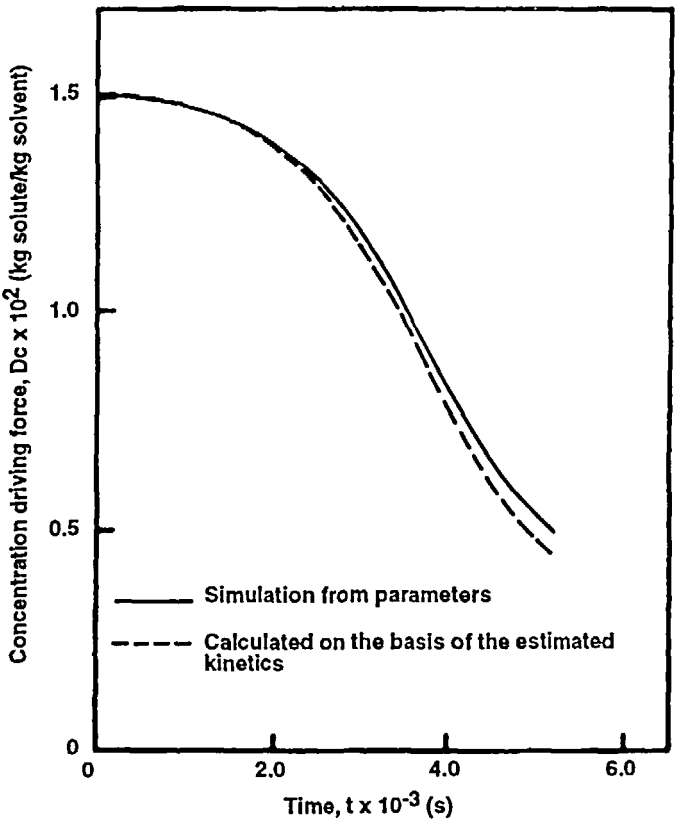

Figure 4 Typical desupersaturation curve (data in Table 4)

numerical methods are now available (see for example Table 4, Tavare[17]). In general the use of analytical solution techniques is restricted to linear systems or to those that can be linearized in some way. Development of a generalized numerical technique to solve the set of equations describing the batch crystallizer configuration is important and relatively little work has been reported in the literature. Garside and Tavare[18,19] developed a numerical algorithm to solve the population balance equation (e.g. equation 16) by the method of numerical integration along the characteristics in conjunction with the supersaturation balance (e.g. equation 24) coupled by the moment

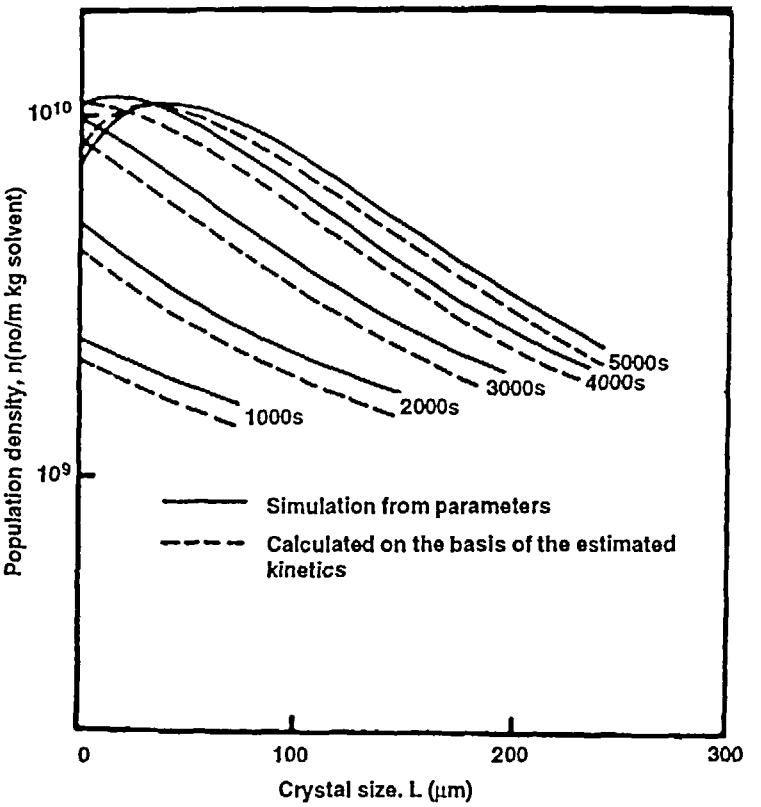

Figure 5 Evolution of population density with time (data in Table 4)

equations (equations 18–21). The resulting desupersaturation curve and the evolution of the size distribution with time, for the particular set of physicochemical parameters listed in Table 4 and calculated by the numerical algorithm using an overall time interval of 1000s for the crystal size distributions, are depicted in Figures 4 and 5 respectively. Again the solid curves represent the numerical solutions obtained using the assumed known kinetic parameters whereas the dotted curves derived from the estimated kinetic parameters. The particular characteristics of population density plot

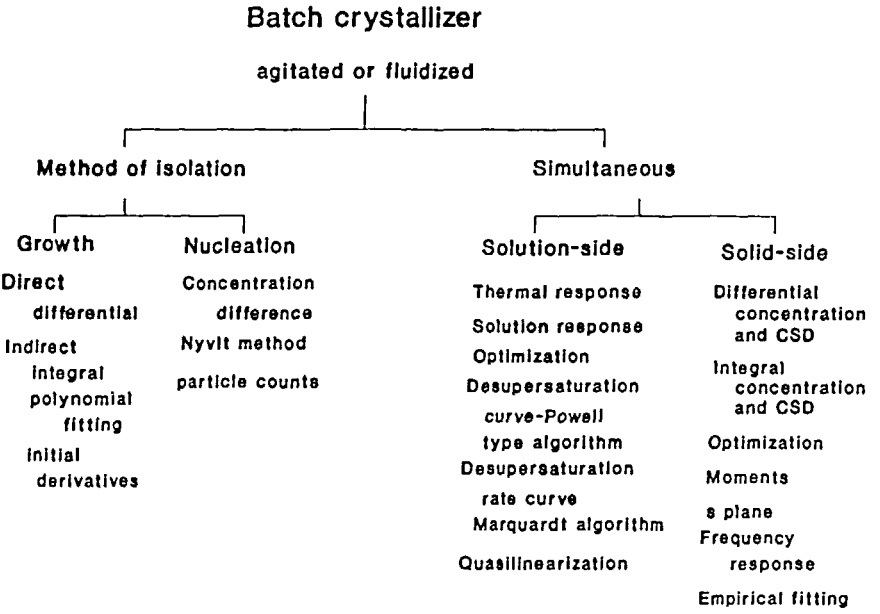

Figure 6 Kinetic data collection techniques

will of course depend on the the specific parameters used in the algorithm. It is rather difficult to solve the population balance equation for complex batch operations especially when nonlinear or higher order terms are included. Special precautions should be taken in handling weak solutions (i.e. solutions with shocks or discontinuities).

5. DETERMINATION OF CRYSTALLIZATION KINETICS

In recent years there has been an increasing recognition to the importance of crystallization kinetics in assessing the design and performance of crystallizers. The characterization of crystallization kinetics in an environment typical of that encountered in industrial situations is therefore of utmost importance. Numerous techniques have been devised to measure and analyze crystal growth and, to a far lesser extent, nucleation. The experimental techniques

developed to extract crystallization parameters as depicted in Figure 6 are based on phenomenological models and are closely related to those used in chemical reaction engineering. The classical approach to establish crystallization kinetics is to isolate the growth and nucleation processes and determine their kinetics separately by direct and/or indirect methods under different hydrodynamic conditions. Several desirable techniques employing simultaneous estimations of all the kinetic parameters in the rate expressions formulated for the associated rate processes using experimental responses are being developed.

5.1 Method of Isolation

5.1.1 Crystal Growth

Direct methods to characterize crystal growth include single crystal studies, measurement of weight gain or movement of a distribution of seeds suspended in supersaturated solution. In an indirect method supersaturation depletion is measured.

5.1.1.1 Single Crystal Studies

A variety of techniques have been reported to carry out single crystal studies (see for example Table 3 in Tavare[1]). Although the information derived from such studies may not necessarily be useful in direct design and analysis of industrial units they indeed provide valuable semiquantitative guidelines for narrowly specialized problems. Good agreement between growth rate results obtained in single crystal and fluidized bed crystallizer studies was observed under carefully controlled conditions of solution velocity and supersaturation[20,21] Klug and Pigford[22] reported a comparable growth behaviour of anhydrous sodium sulphate crystals in two types of experiments viz. single crystal growth studies by photomicroscopic observations in a flow–cell and growth of an ensemble by the transient CSD measurements in isothermal batch experiments. In his correspondence Tavare[23] pointed out that the stochastic distribution of growth rate activities determined from a

large number of single isolated crystals may not necessarily be applicable to an ensemble of growing and nucleating crystals as in the isothermal batch experiments. The consistent definition of an average growth rate for an ensemble of crystals with changing population with time is the time rate of change of total crystal length per crystal and not the time rate of average length of a crystal. Work concerning contact nucleation provides strong experimental evidence of mechanism and also occurrence of growth rate dispersion. The recent spectacular advances in microelectronics have been made possible in part because of the ability to grow single crystals of precisely controlled composition and structural perfection. Crystal size, shape or habit, purity, perfection, strength and abrasion resistance are the parameters that frequently determine the suitability of particular crystal for specific applications and some of them may perhaps be studied on single isolated crystals. Single crystal studies are also important in gaining a better understanding of all synthetic materials especially oxidic ceramics and fundamental information concerning the structural aspects at atomic level and special behaviour of materials by different techniques. For example the critical current density performance of a superconducting material in a single homogeneous form would be significantly enhanced. Inclusion of grain boundaries in a material may cause the critical density to drop drastically.[24] Emphasis in certain applications may change in coming years from multi–particulate CSD studies to single crystal studies.

5.1.1.2 Model Batch Crystallizers

Although a number of techniques have been proposed for growth rate measurements, batch agitated vessel and fluidized bed experiments are being emphasized. For solutions that will sustain moderate to high level of supersaturation useful design insights can be provided by relatively simple laboratory growth experiments. Frequently two different modes of experiments under conditions of negligible mass deposition in nucleation have been used. In a differential mode a small quantity (~0.5 kg/m^3) of closely sized and weighed crystals is allowed to grow for a predecided period. In this type of operation solution concentration changes are small so the crystals grow

at essentially constant supersaturation but at the same time measurable solid deposition is achieved (~1.0 kg/m^3). Direct measurement of the crystal weight changes enables the overall growth rate to be determined as

$$R = \frac{\Delta W}{A_T \Delta t} \tag{27}$$

at a particular temperature, crystal size and supersaturation level. Results of growth rates from several experiments may be correlated in terms of the operating variables.

In the integral mode, on the other hand, a relatively large seed loading (~ 5–10 kg/m^3) of closely sized crystals is charged to the crystallizer. The growth process consumes appreciable solute, thus resulting in decay in supersaturation during the course of an experiment. If the experimental results of supersaturation are empirically fitted into a fourth order polynomial in time as

$$\Delta c = a_0 + a_1 t + a_2 t^2 + a_3 t^3 + a_4 t^4 \tag{28}$$

the desupersaturation rate at a point then is

$$\frac{d\Delta c}{dt} = a_1 + 2a_2 t + 3a_3 t^2 + 4a_4 t^3 \tag{29}$$

When a model crystallizer is operated isothermally with a negligible mass deposition in nucleation and no generation of supersaturation the supersaturation balance (equation 7) at any time in a batch operation is given by

$$R = -\frac{1}{A_T}\frac{d\Delta c}{dt} \tag{30}$$

Using equations (8–12, 28–30) values of growth rate, supersaturation, average size and slurry voidage at any particular time may be obtained. Results from several runs may be correlated in terms of operating state variables such as supersaturation, temperature, crystal size and hydrodynamic situation.

5.1.1.3 Method of Initial Derivatives

Garside et al[25] suggested an elegant technique to evaluate crystal growth kinetics from an integral mode batch experiment. They used a second order polynomial (in time) fitting of an initial portion of a desupersaturation curve obtained in an integral experiment to determine the first two derivatives at zero time. The kinetic parameters in a power law crystal growth rate in terms of mass deposition can be related as

$$g = \frac{2F\Delta c_0}{3\rho_c A_{T0} L_{2,10}} + \frac{\Delta c_0 \ddot{\Delta c_0}}{(\dot{\Delta c_0})^2} = \frac{2Fa_0}{3\rho_c A_{T0} L_{2,10}} + \frac{2a_0 a_2}{a_1^2} \tag{31}$$

$$k_g = -\frac{\dot{\Delta c_0}}{A_{T0}\Delta c_0^g} = -\frac{a_1}{A_{T0} a_0^g} \tag{32}$$

Thus the evaluation of zero time derivatives of a single desupersaturation curve enables the growth kinetic parameters to be obtained directly.

Tavare[26] extended the foregoing analysis to a batch cooling crystallizer and showed that the initial derivatives of the supersaturation and temperature profiles obtained in a series of integral batch experiments can be used to evaluate directly the kinetic parameters(g, E and a) in a crystal growth relation. Although both the techniques are sensitive to experimental errors in the measurements of the initial portions of experimental responses, the results reported[14,25,26] show that the method appears reasonably reliable and the accuracy of the resulting kinetic responses is probably comparable to that obtained using more involved conventional techniques. These techniques certainly increase the experimental ease and flexibility with which the growth kinetics can be determined for many crystallization systems.

5.1.1.4 Growth Rates From CSD

Misra and White[27] have reported a technique in the case of alumina precipitation, following the work of Lyapunov and Kholmogoatseva[28], to

determine the overall linear growth rates from a pair of cumulative number oversize distributions at two times, interval Δt apart for a batch configuration having constant number of total particles and pure convective growth. The growth rate at size L may be defined from the population balance equation (equation 16) for constant solvent capacity system and using the definitions of cumulative number and population density distribution as

$$G = \frac{\Delta N}{\Delta t} \cdot \frac{\Delta L}{\Delta N}\Big|_L = \frac{\Delta L}{\Delta t} \tag{33}$$

5.1.2 Nucleation

Nucleation is the least understood of the two rate processes involved in crystallization, the most difficult to describe by well founded kinetic expressions and the hardest to characterize reliably in a practical situation. Mullin et al.[29] attempted to characterize nucleation rates of potash alum and potassium sulphate in a fluidized bed crystallizer from the difference in solution concentration before and after dissolving nuclei and define the regions of heavy nucleation. This method is very sensitive to solution concentration measurements and unlikely to lead to precise parameter estimates for the nucleation process.

Nyvlt[30] reported a rapid, simple and indirect method to determine the nucleation kinetics in a simple power law nucleation rate expression in supersaturation by measuring the maximum allowable undercooling at a constant cooling rate i.e. the measurement of metastable zone width. In his original treatment the rate of supersaturation generation was assumed equal to that deposited by nucleation process and the slope of the line obtained by plotting the detected undercooling against the cooling rate has been interpreted as the order of nucleation process (i.e. the exponent of supersaturation in power law expression). Several refinements and experimental measurements for a large number of inorganic salts from their aqueous solutions with and without seeds have been reported (see for example Table 3 of Tavare[1]). This method assigns most weight to one characteristic point which is itself very sensitive to the method of detection. Further this

point will generally lie outside the normal working range of supersaturation in a real crystallizer. Hence even though the method is rapid it might lead to unrealistic values of kinetic parameters (see also Janse and de Jong[31], Hiquily and Laguerie[32]).

Misra and White[27] employed the time variations of total number of crystals and concentration to characterize the nucleation kinetics in a batch operated stirred crystallizer for alumina precipitation from caustic aluminate solution. They also incorporated a procedure to evaluate total number of particles down to zero size and used the definition of nucleation rate as

$$B = \frac{\Delta N}{\Delta t} \tag{34}$$

where ΔN is the change in specific cumulative number oversize distribution at $L = 0$ in a time interval Δt. Such an algorithm may however be difficult to use in many other systems in part perhaps due to unreliability of particle size analysis techniques towards the lower size range.

A method of isolating secondary nuclei by removing them from suspension and allowing them only to grow with subsequent characterization by some techniques has been reported in the literature (see e.g. Toyokura et al.[33-34]).

5.2 Simultaneous Estimation

The so–called continuous MSMPR (mixed suspension mixed product removal) crystallizer technique with its simple exponentially decaying steady state CSD

$$n = n^0 \exp(-L/G\tau) \tag{35}$$

has proved the most popular means of quantitatively measuring both the growth and apparent nucleation rate simultaneously. The usual population density plot (ln n versus L plot) should give a straight line for equation (35) with slope $= -1/G\tau$ and intercept $= n^0$. The product of growth rate (G) and nuclei population density (n^0) is the apparent or effective nucleation rate (B).

Analysis of experimental results for the steady state case is simple and the technique has been used by many investigators.[35] Such experiments however have a number of disadvantages. They are time consuming and laborious and often require an elaborate experimental arrangement. A large number of experiments are necessary to elucidate the kinetic expressions as a function of state variables even with minimum number of parameters. It can be difficult to operate a continuous crystallizer under MSMPR constraints because of the problems associated with handling supersaturated solutions and suspensions, especially when toxic and viscous materials are involved. A possibility of segregation does exist in continuous units leading to misleading kinetic information. Further, as the solution holdup requirements is relatively larger, such a technique may not be suitable for expensive fine chemicals.

Some attempts have been made to derive the crystallization kinetics from transients of CSDs from an MSMPR crystallizer.[12,36-43] The methods using transient population density information in an MSMPR crystallizer by themselves appear useful only to provide an independent check on the reliability of the kinetic parameter estimates.

Batch crystallizers may have definite advantages over continuous systems for the determination of kinetics in the laboratory. Motivation for their use is provided by the relative ease with which a large number of operational variables can be studied within a relatively short time. Systems which are difficult to process continuously may conveniently be investigated in a batchwise manner with minimum development time and investment. However the use of batch crystallizers is complicated by the variation with time of both crystal population and supersaturation within the system during the course of experiments. Consequently experimental ease may be partly offset by computational complexity. Again depending upon the type of information made available in a batch experiment, different techniques for simultaneous estimation of crystallization kinetics can be employed.

5.2.1 Solution–side Information

5.2.1.1 Thermal Response

Omran and King[44] used the thermal response, caused by the release of latent heat of crystallization, to establish the crystallization kinetics of ice crystals from sugar solutions and fruit juices by seeding with a single ice crystal. Kane et al.[45] also demonstrated the use of thermal response in an intermediate step of freeze desalination to determine the crystallization kinetics of ice crystals from saline, emphasizing a later portion of the response curve. Stocking and King[46] improved the experimental technique using quartz thermometry so as to achieve the high resolution measurement of initial thermal response. Shirai et al.[47] measured both the thermal response with a highly sensitive thermistor and the crystal size distribution with a microscope during batch crystallization of pure water and of a 5% dextran solution in order to determine the kinetics. The techniques developed in all these studies are restricted to the determination of nucleation characteristics usually based on per crystal, in a dilute crystal suspensions and assign a greater weighting to the characteristic points; these are rather difficult to estimate precisely. Shi et al.[48] in their study of ice crystallization from aqueous solutions in suspension crystallizers for the development of freeze concentration processes suggested that the control over both heat and mass transfer rates is important in order to achieve optimal performance. They followed crystal size distribution and morphology of ice crystals by image analysis of periodic samples. Kyprianidou–Leodidou and Botsaris[49] investigated a process of freeze concentration from sucrose solution by the formation of ice layer on the externally cooled walls in order to minimize the solution entrapment. The formation of the layer was initiated by secondary nuclei induced by rotating ice seeds, at subcoolings smaller than the critical subcooling needed for spontaneous nucleation, yielding smaller entrainement of sugar in ice than that at higher or at the critical subcooling.

5.2.1.2 Solution Concentration

Halfon and Kaliguine[50] investigated the crystallization of alumina from caustic aluminate solution of the second stage Bayer process in an isothermal batch crystallizer by following the concentration variation with time. Kinetic

constants in rate equations were estimated for known kinetic orders with respect to supersaturation from experimental results and attempts were made to discriminate between various mechanistic models using a statistical approach. Verigin et al[51] recovered the crystallization kinetics of potassium dichromate from the experimental concentration profile obtained from a linearly controlled batch cooling crystallizer. Although the technique employed was not described in detail and may be of dubious soundness, high order nucleation (~7) and linear growth kinetics were reported.

5.2.1.3 Non–linear Parameter Estimation

Garside and Tavare[18] examined the possibility of a technique to deduce both growth and nucleation kinetics simultaneously from simulated desupersaturation curves representing the behaviour of seeded isothermal batch crystallizers charged with an initially supersaturated solution and described by equations (7–14) in the section on solution–side process representation. The supersaturation equation is in general a non–linear first order differential equation and its solution represents the variation of supersaturation within the crystallizer with respect to time. This variation, which can be determined from experimental measurements, is a function of time and the kinetic parameters. Determination of the parameters by matching the solution of the non–linear model directly to experimental data results in a non–linear parameter estimation problem. This may be treated as an optimization problem in parameter space in which the dependent variable (Δc) and independent variable (t) have fixed values and the kinetic parameters are variables.

Non–linear parameter estimation procedures implemented by two iterative algorithms (viz. those of Marquardt and Powell) were used. Several optimization techniques are though now available. If Y represents a random observable dependent variable (the response); x a set of several non–random independent (controllable) variables; β a set of parameters in the model and η an expected value of Y at x for given β, then the regression can be represented as

$$Y = \eta(x,\beta) + \epsilon \qquad (36)$$

The function to be minimized for the non–linear least squares problem, i.e. the sum of the residual squares over all the observations may be expressed as

$$F(\beta) = \sum_{i=1}^{m} \epsilon_i^2 \tag{37}$$

where m represents the total number of observations made and must always be greater than the number of parameters.

All the algorithms for non–linear parameter estimation generate an iterative sequence $(\beta^{(k)})$ that converges to the true solution b in the limit. To terminate the computation of this sequence a convergence test is performed to determine whether the current estimate of the solution is an adequate approximation. The recursion relation in the sequence is

$$\beta^{(k+1)} = \beta^{(k)} + \alpha^{(k)} p^{(k)} \tag{38}$$

where $p^{(k)}$ is termed the direction of search and $\alpha^{(k)}$ is the step length. The step length $\alpha^{(k)}$ is chosen so that

$$F(\beta^{(k+1)}) < F(\beta^{(k)}) \tag{39}$$

and may be computed by any one of various methods available. Most algorithms use one of the two approaches. The objective function can be expanded as a Taylor series and the improvements or corrections to the several parameters can be calculated at each iteration on the assumption of local linearity. Alternatively various modifications of the method of steepest descent may be used. Both these approaches not infrequently fail, the Taylor series method because of divergence of successive iterates, the steepest–descent (or gradient) methods because of the very slow convergence after the first few iterations.

Marquardt[52] observed that in practice for elongated ridges these two approaches suggest the direction of search nearly orthogonal to each other and suggested a compromise approach. In his method, at any point β and given

Marquardt parameter λ, the correction or improvement vector δ is obtained by solving the relation

$$(J^T J + \lambda D)\,\delta = -J^T \epsilon \tag{40}$$

where J is the Jacobian matrix of function ϵ and D is a diagonal scaling matrix with non–zero elements. If the sum of squares $F(\beta + \delta)$ is less than $F(\beta)$, then $(\beta + \delta)$ is accepted as the starting point for the next iteration; otherwise λ is increased and the process is repeated. It is interesting to note that equation (40) encompasses both the previous approaches as the limiting cases. When $\lambda = 0$ this method reduces to the first approach of expanding the objective function as a Taylor series while $\lambda \rightarrow \infty$ corresponds to the gradient method. Choices of the initial values for λ, factors by which λ should be changed and decisions on when to change can be made in order to improve the efficiency of the method. Thus by choosing an optimal value of λ at each iteration good progress towards the convergence can be maintained. The selection of λ is based on solution of the normal equations and evaluation of $F(\beta + \delta)$. Marquardt algorithm can be used to match the accumulation term $(-\Delta\dot{c})$ obtained from from the experimental results with that calculated from the right hand side of equation (7) with the current values of the parameters in an iteration and requires the values of the partial derivatives of residuals (ϵ_i) with respect to parameters (β_j) at any time.

A typical iteration of the other hybrid method due to Powell[53] starts with the best possible point known so far β, a step length bound BB, Marquardt parameter λ, and approximation to J and the generalized inverse $[J^T/\sqrt{\lambda}I]^{-1}$ of the matrix $[J^T/\sqrt{\lambda}I]$. These approximations are used to estimate the steps to the minima along the Marquardt and the steepest descent direction. The actual step taken δ, is a linear combination of these estimates chosen so that $\delta < BB$. The residuals are evaluated at $(\beta + \delta)$ and the size of BB is then adjusted according to how successful δ was in reducing the sum of squares $F(\beta)$. The approximation to J and $[J^T/\sqrt{\lambda}I]^{-1}$ are updated so as to be consistent with the changes produced in residuals ϵ by the step δ. The Marquardt parameter λ is initially set to a small value and most iterations

avoid changing it as this would mean the calculation of a new generalized inverse. If however the several iterations as per equation (40) give excessive steps, λ should be increased. The classic features of this algorithm are that it combines both approaches in such a way as to give steady progress and a fast rate of the ultimate convergence but does not require the partial derivatives of the residuals with respect to the parameters. This algorithm is used to match the experimental supersaturation values to the corresponding values obtained from the solution of the supersaturation balance equation (equation 7).

5.2.1.3.1 Exact Responses

5.2.1.3.1.1 Desupersaturation rate curve

The responses as calculated desupersaturation and desupersaturation rate curves in Figures 2 and 3 were used to provide the data points simulating the results of experimental measurements. Thirty data points were taken from the these curves, the time interval between these points being initially 30s, increasing to 510s at the end of the 5400s batch time. The Marquardt algorithm was used to match desupersaturation rates evaluated from the supersaturation balance (equation 7) with the known kinetic parameters (the *model response*) with the *experimental response* represented by the exact data point obtained.

As mentioned before the Marquardt algorithm requires partial derivatives of the residuals in the objective function with respect to the parameters in order to evaluate the Jacobian matrix, J. These partial derivatives of the residuals with respect to the parameters at any time can be evaluated analytically with the help of the regression equation (equation 36) and the supersaturation balance equation (equation 7). Scaling often has a significant influence on the performance of optimization techniques. The residuals in the objective function (equation 37) were therefore multiplied by 10^5, a specific scale factor used for multiplying both sides of equation (7), so that the desupersaturation rates would have values around unity. The properties of the gradient methods are not scale invariant. Use of some standard recommended procedure in δ

space helps in reducing the elongation of the objective function. In the present work this was achieved by setting the elements of the D matrix in equation (40) automatically to the corresponding diagonal elements of the J^TJ matrix at the initial points. Should however the diagonal elements be zero the corresponding elements of D was set equal to unity.

Physical constraints on the parameters can be incorporated into the Marquardt algorithm. The rate constants were constrained to have non–zero positive values while the kinetic orders were subject to lower and upper bound of 0 and 15 respectively. If the value of a parameter violated the imposed constraint, the residuals were not calculated but the iteration was repeated with the larger value of the Marquardt parameter λ causing a smaller improvement in the parameters. Such changes in λ should be confined to early iteration only indicating successful avoidance of the constraints. If however the changes persist throughout the computation the routine may converge to a minimum on, or very near, a constraint.

An iterative Nag Library subroutine was used to implement the Marquardt algorithm. In each iteration the desupersaturation rate was evaluated from the supersaturation balance (equation 7) which was integrated numerically with the improved values of the parameters evaluated in the previous iteration so as to obtain the values of Δc. This gave the model response which was then compared with that taken from the measured desupersaturation curve (*the experimental response*). The convergence test used was that the improvement vector should be equal to or less than the specified limits. The limits used on the rate constants and the kinetic orders were $1x10^{-7}$ and $1x10^{-5}$ respectively and were much lower than those acceptable in practice. These gradients should be sufficiently zero at the convergence point. It is also necessary to show that the convergence is achieved at one unique point, probably the global minimum for wide range of initial parameter estimates. The parameters corresponding to this point are in general very close to actual values. In the present case it was a true convergence. Values of the multiple of the gradient of the sum of error squares function (i.e. the elements of the $J^T\epsilon$ matrix) also provides independent information regarding convergence. These values were $< 1x10^{-15}$ which are sufficiently close to zero as compared to the residuals ($\sim 10^{-9}$) at the point of convergence as indicated by the solid curve in Figure 3.

5.2.1.3.1.2 Desupersaturation curve

The hybrid algorithm due to Powell was used to match the supersaturation values (*the model response*) evaluated from the supersaturation balance (equation 7) with the exact supersaturation values (*the experimental response*) represented by data points (Figure 2) at the same time intervals as used for the desupersaturation rate curve. An estimate of the Euclidean distance (STEPMX) between the expected minimum and the starting point of the β on which steplength bound BB was based was assigned to be unity and should preferably have higher value ($\sim 10^3$–10^4) in some cases for better resolution. Analytical functional forms of the partial derivatives of residuals with respect to the parameters were not required in the Powell algorithm. A suitable step length (h) for making the difference estimates of the partial derivatives needed to be specified. The step length had to be small enough for the difference estimates to be close to the time derivatives but not so small that the calculated differences were dominated by the rounding errors. The particular value specified in this work was equal to the square of the machine accuracy.

The algorithm used STEPMX to control the length of the steps and h to calculate the differences. For both these processes it was important that the parameters (β) should be scaled (by multiplying them by appropriate constants) so that their magnitudes were similar. In the present case nucleation rate coefficient k_b was scaled in such a way that would have a numerical value of around 5. The iterative hybrid Powell algorithm was implemented via a library subroutine to this problem. In each iteration the supersaturation balance (equation 7) was integrated numerically using the improved values of the parameters estimated in the previous iteration. The numerical integration was performed using the fourth order Runge Kutta subroutine with a step length of 30s to evaluate the model response. It was then compared with the experimental response. The convergence test used was that the difference in the values of the sum of error squares functions in two successive iterations should be equal to or less than a specified quantity. The choice of this convergence test was important because it was also used as a lower bound for the Marquardt parameter. The accuracy on the difference is limited by that of the machine and the order of the magnitude of sum of error

squares function should be considered. The results indicated that the convergence was achieved at a point very close to actual values of the parameters, even when widely different initial estimates were used. It was always necessary to ensure that the algorithm achieved a global minimum at or very close to the actual parameter values.

The computational time required for these routines in general depends on the number of parameters, the number and behaviour of functions, the distance of the solution from the starting point and the accuracy of the solution demanded. The number of operations performed in most iterations of the Marquardt algorithm is roughly proportional to the cube of the number of the parameters to be determined. In addition to this, each iteration should evaluate ϵ at β, $\mathbf{J}^T\mathbf{J}$ and $\mathbf{J}^T\epsilon$. Should these evaluations be lengthy the run time will probably be dominated by these computations. The CPU time used by the Marquardt algorithm for a run of about 100 iterations in this problem was around 40s on CDC 7600 machines.

The number of operations carried out in one iteration of the Powell algorithm is roughly proportional to the product of number of observations and the square of the number of parameters to be estimated. In each iteration of this routine ϵ of β needs to be evaluated and the run time will probably be dominated by the time spent in evaluating ϵ. The CPU time required by this routine for a run of about 100 iterations ranges from 150 to 200 s on CDC 7600 machines. The higher CPU time per iteration is probably attributable to the fact that the Powell algorithm uses the difference estimates of the partial derivatives of the residuals with respect to parameters by the forward difference method. The compilation time used by both these routines is however the same (~ 6–7s).

Starting from the same initial point and demanding more or less similar levels of accuracies for typical runs of this problem indicated that although the number of iterations are roughly the same, the CPU time taken by the Powell algorithm is higher than that used by the Marquardt algorithm. These algorithms were found to be robust for the present applications as in most cases with widely different initial guesses true convergence was achieved.

The parameter estimate results obtained in the present synthetic problem do not provide any information about their reliability and precision. The covarience matrix of the probability distribution which is generally assumed to be normal for a sufficiently large number of observations is a measure of the reliability of the estimates. The diagonal elements of this matrix are the variance and hence their square roots are the standard deviations of the parameter estimates. A measure of the precision of the estimates is usually expressed by confidence limits which are simply the product of a fixed number (depending upon the percentage level) and the standard deviation (see Figures 1 and 2 for typical results). These results in general reveal that the kinetic orders can be estimated with greater precision than the rate constants. For certain cases the Marquardt algorithm provided poor reliability, yielding large values for the 95% confidence limits for rate constants and the final sum of error squares of the residuals. The Powell algorithm seems to provide reasonable precision and reliability in this application. A necessary and sufficient condition for the parameter observability is that the Hessian matrix ($\mathbf{J}^T\mathbf{J}$) must be nonsigular, i.e. the elements of the matrix of second partial derivatives of the residuals with respect to parameters, $\frac{\partial^2 \epsilon(\beta)}{\partial \beta_i \partial \beta_j}$, must be positive semidefinite at the minimum of the residuals and is usually satisfied.

The success of the Marquardt algorithm depends on the availability of reliable estimates of *desupersaturation rates.* It would be advantageous if an experimental technique could be devised to provide directly the desupersaturation rates as an experimental response in addition to supersaturation values. Deduction of desupersaturation rate data from an empirical fitting of the experimental supersaturation–time data (*desupersaturation curve*) were found not to be reliable or satisfactory. Although the Marquardt algorithm is efficient the problems associated with measurements may limit its utility in kinetic parameter estimation of this kind.

The quasilinearization algorithm is the other technique among the most common methods that are used in off–line parameter estimation in systems described by sets of ordinary differential equations and are very important in process modelling, simulation and optimization.[54,55] The algorithm is best

known for its fast quadratic convergence to the optimum, but a major problem is its small region of convergence.[56,57] Although several other approaches have been suggested to overcome the small region of convergence[58-64] it appears difficult to get satisfactory results with either solution–side or solid–side description because of very small region of convergence in a parameter space.

5.2.1.3.2 Noisy and Experimental Responses

5.2.1.3.2.1 Desupersaturation curve

The Powell algorithm appears superior to that of Marquardt for reliability and accuracy of the parameter estimates from the exact data point. Error was introduced into the concentration values at these points using a random number generator, different distributions of error being obtained by using different statistical distributions. The standard deviation of these points about the exact values was varied. These data points were used to represent the results of the experimentally measured desupersaturation curves. The Powell algorithm was used to estimate the kinetic parameters. The results indicated the kinetic orders can be estimated rather more easily than the rate coefficients. The best estimates of all four parameters were close to the true values for concentration standard deviations up to about 10^{-5} kg/kg solvent, the estimates of the 95% confidence limits of the rate coefficients were large at this point. On the other hand at the same level of concentration standard deviation the estimates of the orders were reasonably reliable. Experimental determinations of solution concentration imply that the crystallization kinetic orders can probably be estimated using the technique but that estimates of rate coefficients may be unreliable. Application to experimental isothermal desupersaturation curves for potash alum from a 30 L seeded batch crystallizer gave consistent estimates of the kinetic parameters. High order nucleation kinetics probably reflect the high levels of supersaturation used during the experiments.[18]

Palwe et al.[14] determined the best estimates of kinetic parameters in equation (7) from the experimental curves using a comprehensive algorithm for the

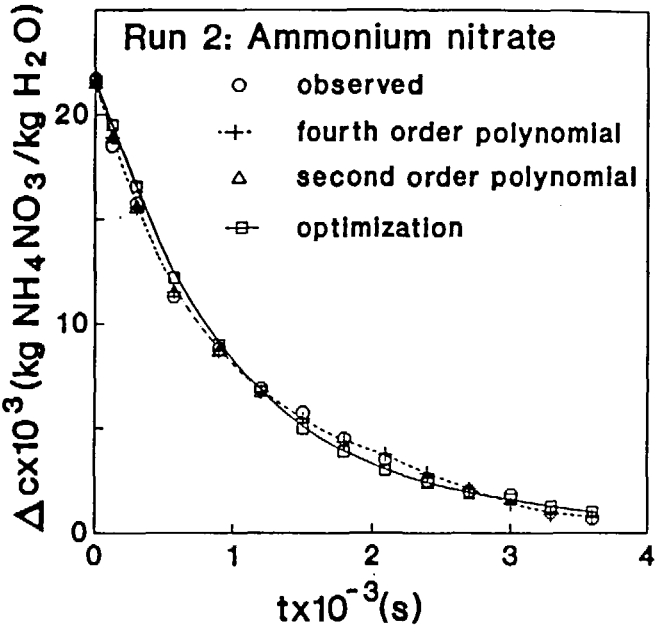

Figure 7 Desupersaturation curve for ammonium nitrate

non–linear least squares problem available as a computer library subroutine (subroutine LSQNDN in NPLA or NAG library). This subroutine has better computational features than, and was included as a replacement for, the Powell algorithm. The routine works for functions having continuous first and second derivatives which are normally evaluated numerically and yields better results even with occasional discontinuities in the derivatives. The step length $\alpha^{(k)}$ as given in sequence of points (equation 38) is usually chosen such that $F(\beta^{(k)}+ \alpha^{(k)})$ is approximately minimum with respect to $\alpha^{(k)}$. The vector $p^{(k)}$ representing a direction of search depends on the reduction in the sum of the residual squares obtained during the last iteration. If the sum of the residual squares was sufficiently reduced then $p^{(k)}$ is an approximation to the Guass–Newton direction; otherwise additional function evaluations are made so as to enable $p^{(k)}$ to be made a more accurate approximation to the Newton direction. Although the method is designed to ensure that steady progress is

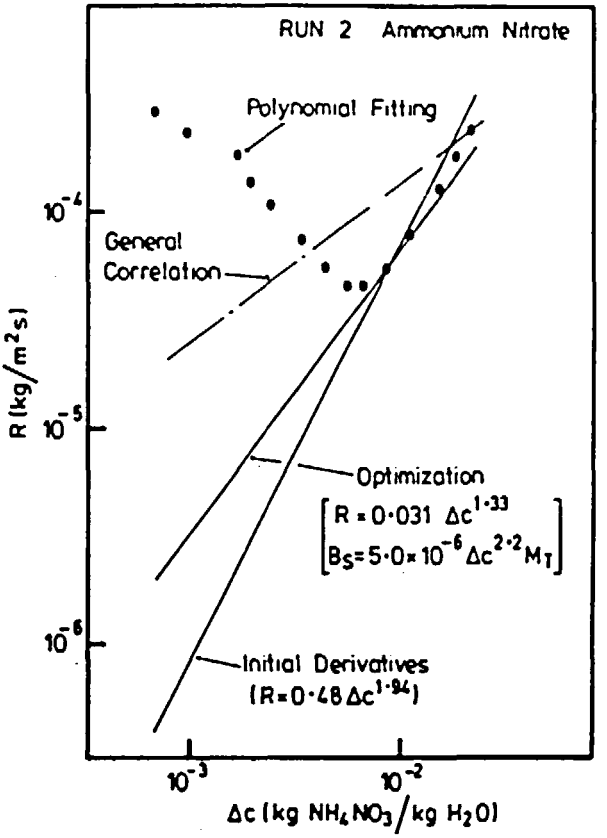

Figure 8 Growth rate data for ammonium nitrate

achieved whatever the starting point and to have a rapid ultimate convergence of the Newton method it was difficult to achieve true convergence for these experimental runs even after reasonable relaxation in the convergence test. The best estimates were selected with the best possible minimum sum of residual squares through several trials with a fixed number of iterations. A typical experimental desupersaturation curve for ammonium nitrate and its optimization and polynomial fitting are shown in Figure 7. The results of growth rate data as a function of supersaturation for the desupersaturation response in Figure 7 are reported in Figure 8 for three techniques viz.

polynomial fitting, initial derivatives and optimization procedures. Also included in Figure 8 is the general growth rate correlation at T = 305 K, ϵ = 0.997, L = 700 μm, N = 10 rev/s deduced from the results of ten experiments. In general the agreement among the three calculation methods are depicted by the representative of the results in Figure 8, is best at high values of supersaturation which corresponds to the initial part of the experiment. The method using the optimization procedure used for the non–linear parameter estimation makes use of all the experimental data points and determines simultaneously growth and nucleation kinetics as in equation (7) for a run. The technique based on initial derivatives utilizes only the initial part of the desupersaturation curve. The growth rate data obtained from the polynomial fit show a reverse trend after some initial period in all the runs because of the change in direction of the supersaturation rate. The techniques of empirical polynomial fitting have been conventionally used in the past but may not necessarily yield consistent growth rate data over the entire range of supersaturation, particularly at low supersaturation level. The method using initial derivatives is the simplest of all and appears sensitive to measurement of the initial supersaturation decay. Although the parameter estimates in kinetic relations were not entirely consistent among the different techniques the kinetic responses calculated from these correlations were comparable over the experimental range. The methods using the optimization procedures are the most accurate and precise they demand inordinate computation time and complexity when an iterative algorithm has to be adopted.

Qiu and Rasmuson[65,66] used a non–linear parameter estimation procedure to extract growth and dissolution characteristics of succinic acid crystals in a batch agitated vessel from the measured desupersaturation. They minimized the sum of error squares of supersaturation residuals defined as the difference between the calculated and measured values. They used the time variation of supersaturation incorporating the growth rate correlation in the integrated definition of the growth rate valid for an ensemble with constant population to calculate the value of supersaturation at any time. In addition to desupersaturation information for non–linear parameter estimation by optimization techniques from a seeded batch crystallizer Witkowski et al[67] suggested that obscuration, a light scattering measurement by a Malvern

particle size analyzer, provides a measure of the second moment of the crystal size distribution and can be used along with the solution concentration data in identification of all the kinetic parameters. Rawlings et al[68] reviewed model identification and control techniques for solution crystallization processes. Measurement technology for on–line crystal size distribution (CSD) and numerical methods in light of parameter estimation procedures were assessed.

5.2.2 Solid–side Information

The use of batch crystallizers for the simultaneous estimation of growth and nucleation parameters appears to have been first reported by Bransom and Dunning[69] They suggested an elegant experimental technique to determine the kinetics of cyclonite precipitation in a batch agitated vessel in a differential mode at different initial supersaturation levels. Misra and White[27] employed the time varying particle size distribution and concentration variation in a non–uniformly seeded isothermal alumina crystallizer and determined the growth rates by following the movement of the size distribution with time and nucleation rate from the particle count.

Wey and Estrin[70] modelled a batch agitated crystallizer for the ice–brine system to determine the crystallization kinetics using the population balance equation coupled with mass and energy balance equations. A general size dependent growth model based on diffusion controlled growth mechanisms and a simple power law for the nucleation rate involving the supersaturation and total surface area were included. In their later work Estrin et al[71] used an orthogonal polynomial of third degree with an exponentially decaying weighting function to simulate the population density function in a batch agitated crystallizer. They thought the hump or the plateau in the conventional population density plot may be due to competition for the dissolved solute between the growth and nucleation processes and used this characteristic in revealing these kinetic parameters. Lee[72] suggested a technique of characterizing both nucleation and growth from the population density response of a stirred batch crystallizer seeded by a single crystal. Wey and Terwilliger[73] in their correspondence have however pointed out the basic

inadequacy in Lee's approach[72] as he assumed constant values of both time varying overall linear growth rate and birth function in a non–programmed batch operation.

Harano and Yamamoto[74-75] attempted to investigate the impurity effects on crystallization kinetics by characterizing both growth and nucleation kinetics for L–glutamic acid crystals by following the transients of light transmittance and electrical conductivity of solution and by CSD analysis of product crystals.

Gutwald and Mersmann[76] measured crystallization kinetics of potash alum in a controlled cooling batch crystallizer maintained at a constant level of supersaturation by using a programmed temperature profile. The variation of solute and magma concentrations were monitored. The change of crystal number with time gives the nucleation rate. They showed that the kinetic results from batch experiments were in good agreement with those obtained in several MSMPR crystallizer studies. Molner et al[77] illustrated a calculation method to extract size dependent growth kinetics of potash alum crystals from a batch cooling crystallizer using the population balance approach.

The population balance equation (e.g. equation 16) is in general a non–linear first order partial differential equation (PDE). Two factors tend to complicate the PDE parameter estimation problem as compared with that for ordinary differential equations (ODEs). First parameters may enter into the boundary conditions as well as into the equations themselves. Second the measurements are functions of both space and time. Thus the experimental data can be either values of state at a certain location or integrated values of the state over some or all of the special domain of the process.

Seinfeld[78] and Seinfeld and Chan[79] developed several non–sequential techniques of the parameter estimation in non–linear PDEs and boundary conditions from noisy experimental data. Alternatively the partial differential equation may be transformed into a set of differential equations by moment transformation and then the problem may be converted into the ODE parameter estimation problem. A rather special situation arises when the

differential equations are linear in which case either the analytical solution or the transfer function can be made available. If the analytical solution is available the parameter estimation reduces to one involving an algebraic model. If the transfer function is available optimization in transformed domain may be used.

Although methods using optimization procedures, as mentioned before, are potentially the most accurate and precise they demand inordinate computation time and complexity when iterative techniques have to be adopted. In addition most iterative algorithms cannot be used as a blackbox for a given parameter estimation problem. The users must know both the technique and the problem well to get the satisfactory results. Because of these limitations Garside and Tavare[18] developed several simplified algorithms to extract the kinetic parameters from population density information.

5.2.2.1 Method of Moments Analysis

The use of moments in system response analysis for parameter estimation in linear models involves matching moments of the system model output to like moments of experimental data. The kth moment of the population density distribution about the origin, obtained by moment transformation with size, is defined as

$$\mu_k = \int_0^\infty nL^k dL \tag{41}$$

If the moments of the experimental population density function are available at two times differing by a small time interval Δt over which the linearity of the model may be assumed, the kinetic parameters can be expressed in terms of moments with respect to size at an average time as

$$\bar{B} = \Delta\mu_0/\Delta t \tag{42}$$

and

$$\bar{G} = \Delta\mu_1/\bar{\mu}_0\Delta t \tag{43}$$

or

$$\bar{G} = \Delta\mu_2/2\bar{\mu}_1\Delta t \tag{44}$$

where Δ represents the difference in values of a quantity at two different times and the bar an arithmetic average of the quantities. These three relations are derived from the moment equations for N crystals (equations 18–21) by converting the derivatives in the differential equations into differentials. Thus the average nucleation rate $\bar{B}$ and average overall linear growth rate $\bar{G}$ may be determined from two experimental population density plots obtained during the course of a batch experiment at times t and $t+\Delta t$. The moments analysis was carried out using exact numerical solution and simulated responses according to Coulter counter particle size analyzer with and without superimposed noise![19] Their simulation studies showed that the results of parameter estimates are not very sensitive to the experimental noise and numerical integration technique employed in evaluations of moments. Generally parameter estimates based on the higher order moments show larger scatter than those based on the lower order moments. A large scatter of all these estimates compared to actual values was identified with the error associated with tail effects.

5.2.2.2 Method of s plane Analysis

It is often advantageous to estimate model parameters in the Laplace transform domain rather than the time domain. Experimentally determined population density can be converted into the Laplace transformed response with respect to size as

$$\bar{n}(t,s) = \int_0^\infty \bar{n}(t,L)\exp(-sL)dL \tag{45}$$

The Laplace transformation of the population balance equation (equation 16) with respect to size yields

$$\frac{d\bar{n}(t,s)}{dt} + G[s\bar{n}(t,s) - n(t,0)] = 0 \tag{46}$$

Although G and n(t,0) are functions of t they can be assumed constant over a small time interval Δt and the parameters will then have an average value over this interval. Using zero initial condition with regard to the initial size distribution for N crystals, equation (46) reduces to

$$\frac{d\bar{n}(t,s)}{dt} + \bar{G}s\bar{n}(t,s) - \bar{B} = 0 \tag{47}$$

Transforming the derivative in equation (47) into differentials gives

$$\frac{\Delta \bar{n}(t,s)}{\Delta t} = -\bar{G}s\overline{\bar{n}(t,s)} + \bar{B} \tag{48}$$

where $\Delta\bar{n}(t,s)$ is the difference between the Laplace transformed population densities at time t and $t+\Delta t$ and $\overline{\bar{n}(t,s)}$ the average of these quantities. In the method of s plane analysis a plot of time rate of change of the Laplace transformed population density against the product of the Laplace transform variable and average Laplace transformed population density over an optimal range of Laplace transform variable will yield a straight line with slope $= -\bar{G}$ and intercept $= \bar{B}$. Thus equation (48) can be used to determine the kinetic rates from a pair of population density curves at two times Δt apart.

One of the obvious advantages of using the Laplace domain is that the sensitivity to experimental errors in the determination of the experimental response is greatly reduced provided that a suitable value of the Laplace transform variable s is used. Clearly, if the value chosen for s is too small then the tail of the response will be heavily weighted whereas if it is too high then too much emphasis will be given to the front portion of the response. In either case a poor estimate of the weighted moments will result. Between these two limits there will be an optimum value of s which reduces the errors due to uncertainties at either end of the response and yet gives weighted moments containing useful information about the system. In general the optimum values of s depends on the mean of the responses, the order of the moments involved in the parameter estimation and the noise sensitivity along the response. Selection of the optimum Laplace transform parameter in the analysis of the crystal growth dispersion in a batch crystallizer has been reported![18]

In formulating the linear regression to estimate $\bar{B}$ and $\bar{G}$ from equation (48) the limits on the optimal values of s must be known *a priori.* Simulation studies[18] indicate that the limits on the values of s should be constrained by $s_f\bar{L}_2 \sim 1$–2 where $\bar{L}_2$ is the population average size at time t_2. The level of error introduced on the simulated response has little effect on the kinetic parameter estimates determined. The method of s plane analysis thus appears to eliminate many of the limitations associated with the method of moments and provides a simple, reasonably accurate and seemingly reliable technique by which to extract parameter estimates from the experimental observations.

5.2.2.3 Method of Frequency Analysis

Frequency response testing is another classic technique used for parameter estimation and design in linear control systems. The frequency response transfer function of a stable linear one dimensional system to any forcing function is simply the Fourier transform with respect to size of the time domain response (or the Laplace transform with $s = j\omega$ in equation 45). Thus

$$\bar{n}(t,j\omega) = \int_0^\infty n(t,L)\exp(-j\omega L)dL \tag{49}$$

or a complex sum of Fourier Sine or Cosine transforms

$$\bar{n}(t,j\omega) = \int_0^\infty n(t,L)\cos(\omega L)dL - j\int_0^\infty n(t,L)\sin(\omega L)dL = \overline{C} - j\overline{S} \tag{50}$$

Transformation of the population balance equation (equation 16) by taking the Fourier transform with respect to size, writing the resulting transforms and separating real and imaginary parts we get the following equations

$$\frac{\Delta\bar{C}}{\Delta t} = -\bar{G}\omega\overline{S} + \bar{B} \tag{51}$$

and

$$\frac{\Delta\bar{S}}{\Delta t} = \bar{G}\omega\bar{C} \tag{52}$$

Over the optimum range of transform parameter ω, a plot of $\Delta\bar{C}/\Delta t$ versus $\omega\overline{S}$ in equation (51) should yield a straight line with gradient = $-\bar{G}$ and intercept = $\bar{B}$ whereas a straight plot of $\Delta\bar{S}/\Delta t$ against $\omega\overline{C}$ in equation (52) should pass through the origin and have slope = $\bar{G}$. Thus equations (51–52) can be used to determine the kinetic parameters if the Fourier Sine and Cosine transforms of the two experimental population density curves separated by Δt apart are available.

5.2.2.4 Methods Based On Empirical Fittings

An experimentally observed response can be fitted to a suitable functional form which then can be used either to extract kinetic parameters or to relate the kinetics parameters in terms of empirical constants. In this section two semi–empirical approaches used in the past will be assessed critically for possible use in the simultaneous estimation of crystallization kinetics parameters.

An approach of using empirical fitting of observed population density response as presented by Sowul and Epstein[41] for sugar crystallization in an MSMPR crystallizer may be considered for a batch crystallizer. The population density function may analogously be represented for a batch crystallizer as

$$n(t,L) = c'\exp(-a'L)\exp(-b'\tau/t) \tag{53}$$

where a', b' and c' are empirical constants and τ is the run time. From the population balance equation (equation 16) and equation (53) the growth rate may be expressed as a function of time by

$$G = -\frac{\partial n}{\partial t} \Big/ \frac{\partial n}{\partial L} = \frac{b'\tau}{a't^2} \tag{54}$$

While putting L = 0 in equation (53) the nuclei population density is given by

$$n^0 = n(0,t) = c'\exp(-b'\tau/t) \tag{55}$$

Thus a', b' and c' can be determined by fitting the observed population density data at any time, t the kinetic rates (G, n^0 and hence B) can be simultaneously determined. In this approach the functional form of equation (53) is assumed to be an analytical solution to the population balance equation (equation 16).

Hulburt and Katz[80] presented an elegant method using orthogonal expansion of the original associated Laguerre polynomials based on a gamma distribution to recover an approximate distribution function from a set of leading moments. Instead of a gamma distribution an exponential function (which is a special case of gamma distribution) may be used for the batch crystallizer. Randolph and Larson[16] have however pointed out that the addition of higher order corrections involving the Laguerre polynomial terms exacerbates the degree of fit by producing increased numerical oscillations thus making the method of no practical value. The use of lower order terms only may yield reasonable results in some cases. Estrin et al[71] used third degree orthogonal polynomials using identical series expansion for fitting the population density response obtained from a batch ice crystallizer. The use of methods based on empirical fittings of the experimental response may be valuable in a specific applications but their generality may be highly questionable.

Previously reported results of population density as a function of size at various times from the two types of experiments were used to check the potentialities of first two of the techniques. The first type of experiment consisted of measuring the desupersaturation curve and population density as a function of size at various time intervals from a 4 L seeded isothermal batch crystallizer charged with initially supersaturated solution for alumina crystallization. The size distribution measurements were made with a Coulter Counter and population density plots were reported in Figure 5 and 10 of the original paper by Misra and White[27] The experimental results were originally used to characterize the growth and nucleation kinetics simultaneously by using numerical differentials. The results of reanalysis of two sets of the original data (Figures 5 and 10; Misra and White[27]) by two methods viz. moments and s plane analysis are reported in Table 5. The values of growth and nucleation rates are in most cases not only consistent among themselves

Table 5 Crystallization kinetics of alumina from a batch crystallizer (Misra and White[27])

Fig no. in ref 27	process variables	time internal min	moments analysis $\bar{G}x10^{10}$ m/s eq 44	moments analysis $\bar{G}x10^{10}$ m/s eq 43	moments analysis $\bar{B}$ no/smL eq 42	s plane analysis $\bar{G}x10^{10}$ m/s ←eq 48→	s plane analysis $\bar{B}$ no/smL ←eq 48→	s plane analysis r % ←eq 48→
5	T = 75°C	0–160	10.6	17.5	$1.2x10^{3}$	24.9	$1.2x10^{3}$	99
	W_0= 10g/L	160–340	8.1	8.2	$1.x10^{11}$	8.2	–0.62	99
		340–1875	0.6	0.6	$1.x10^{12}$	0.6	–0.002	100
10	T = 60°C	0–270	3.1	3.5	$1.7x10^{3}$	3.9	$1.7x10^{3}$	99
	W_0= 10g/L	270–420	3.7	4.6	$3.7x10^{3}$	5.4	$3.7x10^{3}$	99
		420–1170	0.6	1.0	$2.1x10^{3}$	1.3	$2.1x10^{3}$	99

but also are comparable with those reported in the original paper ($\bar{G} \sim 2–10x10^{-10}$ m/s and $\bar{B} \sim 0–5x10^{3}$ no/s mL).

In the second type of experiment a 48 L seeded batch cooling crystallizer was operated at a predetermined cooling rate using an electronic temperature control system. Two systems, potassium dichromate and potash alum, were used for the experiments and the results in the form of population density as a function of size at various times derived from sieve analysis were reported. The results obtained using the two parameter estimation procedures and data from original figures (Figure 7.1, page 89; Figure 7.18, page 106; Janse[81]) are presented in Table 6. In most cases the results for both these systems show consistency among themselves and are reasonably comparable with those reported previously (potassium dichromate: $\bar{G} \sim 3–10x10^{-8}$ m/s, $\bar{B} \sim 10^{6}–10^{8}$ no/s t or no/s 1000 kg (Janse[81]); potash alum: $\bar{G} \sim 1–10x10^{-8}$m/s, $\bar{B} \sim 10^{7}–10^{8}$

Table 6 Crystallization kinetics of potassium dichromate and potash alum from a batch cooling crystallizer (Janse[81])

Run no	Fig no in ref 81	stirrer speed rev/min	time intervals min	moments analysis $\bar{G}x10^{8}$ m/s eq 44	moments analysis $\bar{G}x10^{8}$ m/s eq 43	moments analysis $Bx10^{-6}$ no/st eq 42	s plane analysis $\bar{G}x10^{8}$ m/s ←eq 48→	s plane analysis $Bx10^{-6}$ no/st ←eq 48→	r % ←eq 48→
Potassium dichromate–water system ($\dot{T}$ = 10°C/h, T_0 = ~40°C, T_f = ~20°C, M_T =~.2–115 kg/t, τ = 100 min)									
7	7.1	1200	0– 8	15.3	19.8	9.3	24.9	9.6	99
			8– 52	2.3	3.1	4.8	4.1	5.0	99
			52–105	1.3	2.2	10.9	3.2	11.4	99
9	7.1	500	0– 8	22.0	32.0	6.6	44.5	6.8	99
			8– 48	4.7	3.5	0.4	2.8	0.4	99
			48–103	1.7	1.9	1.2	2.3	1.2	99
17	7.1	1000	8– 50	2.6	3.4	2.5	4.4	2.5	99
			50–105	1.3	2.0	3.5	2.8	3.7	99
Potash alum–water system ($\dot{T}$ = 10°C/h, T_0 = ~38°C, T_f = 22°C, M_T = ~30–125 kg/t, τ = ~80 min)									
3	7.18	500	8– 30	3.1	3.1	6.8	3.1	6.8	99
			30– 80	1.4	1.3	4.4	1.2	4.4	99
10	7.18	250	10– 28	3.1	2.9	8.0	2.9	8.0	99
			28– 82	1.2	1.3	7.7	1.5	7.9	99
12	7.18	1000	8– 36	2.2	2.2	15.3	2.2	15.4	99
			38– 86	1.3	1.7	27.8	2.2	28.8	99

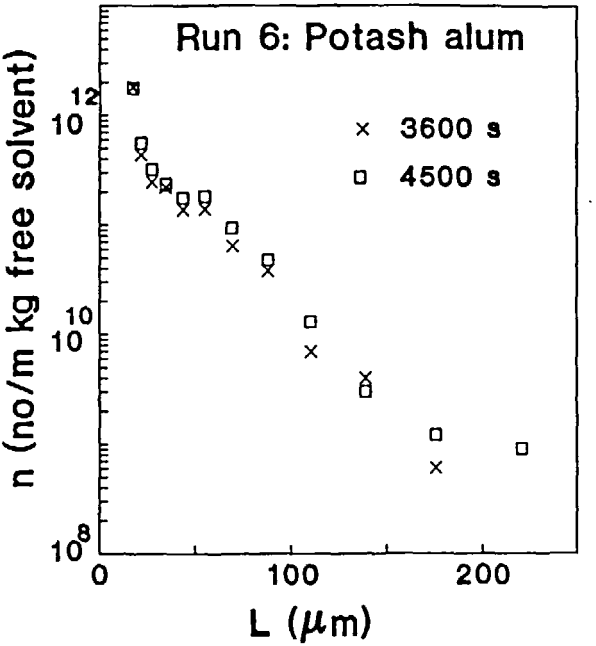

Figure 9 Population density data from a batch crystallizer

no/m^{3}s (Jancic[82])). In assessing these results it is necessary to note the original data used in the calculations were obtained from experiments that were not specifically designed to use the parameter estimation procedures.

Garside and Tavare[18] have examined critically all these simplified parameter estimation procedures using simulated experimental observations of the population density to judge their suitability. The method of s plane analysis was found satisfactory. A typical pair of population density curves obtained in an experiment performed with potash alum in a 25 L seeded, isothermal draft tube baffled agitated crystallizer is shown in Figure 9 and the resulting linear plot in equation (48) for the method of s plane analysis using the experimental data is given in Figure 10.

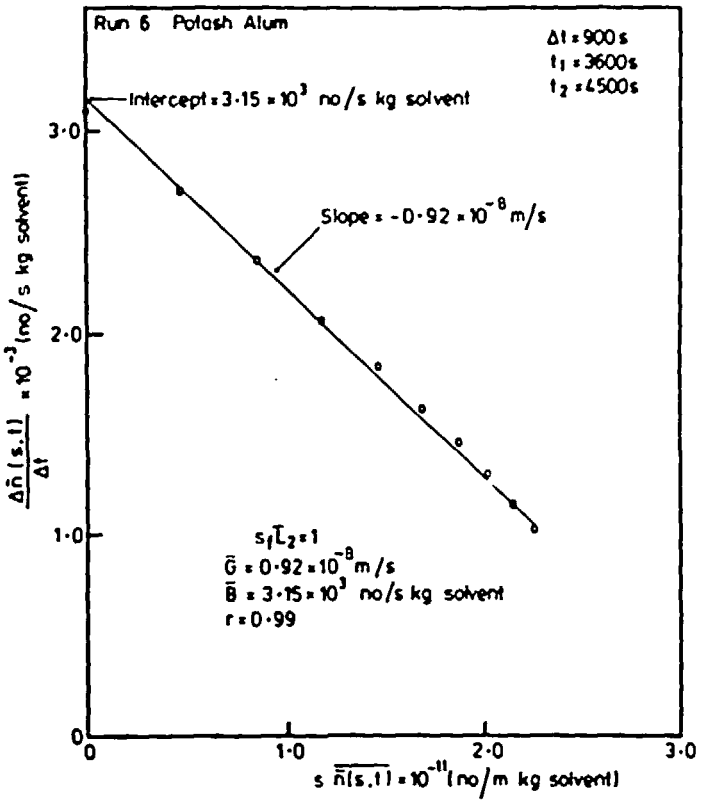

Figure 10 The method of s plane analysis for data in Figure 9

Several studies have been performed using the most suitable technique out of simplified parameter estimation procedures viz. the method of s plane analysis. Although the parameters in the kinetic relations resulting from all these studies were not entirely consistent with those previously reported for the corresponding systems measured using the other conventional techniques (e.g. continuous MSMPR crystallizers) the kinetic responses calculated from the different correlations were comparable over the range of experimental variables. The comparison of growth and nucleation rates, for example, in Figure 11, shows that the correlations by the method of s plane analysis give

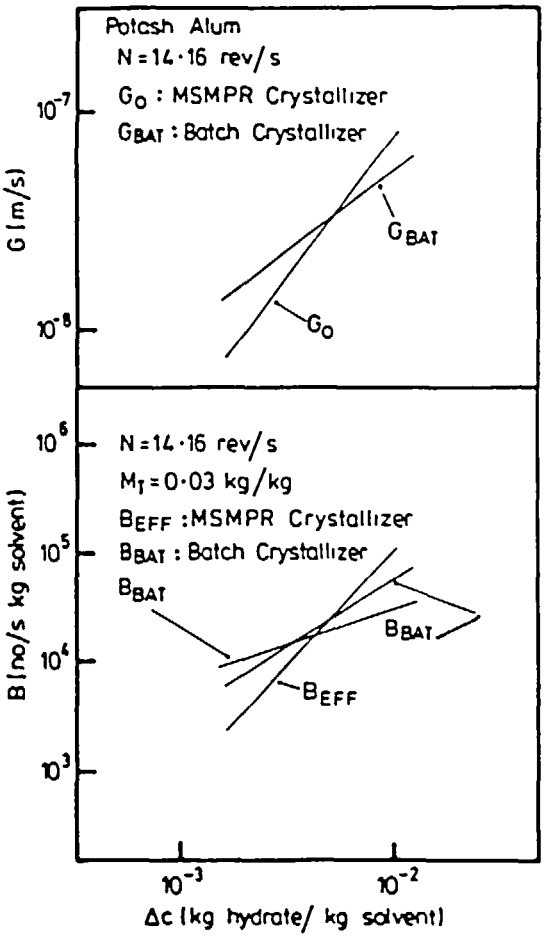

Figure 11 Comparison of growth and nucleation kinetics

similar rates to those of Garside and Jancic[83] determined from continuous MSMPR crystallizer with size distribution measurements down to about 35 μm. There is also consistency between the two nucleation correlations for batch studies determined as a function of growth rate and supersaturation. The kinetic responses calculated from the different correlations as reported in Figures 12 and 13 appear consistent with the range of size distributions used in

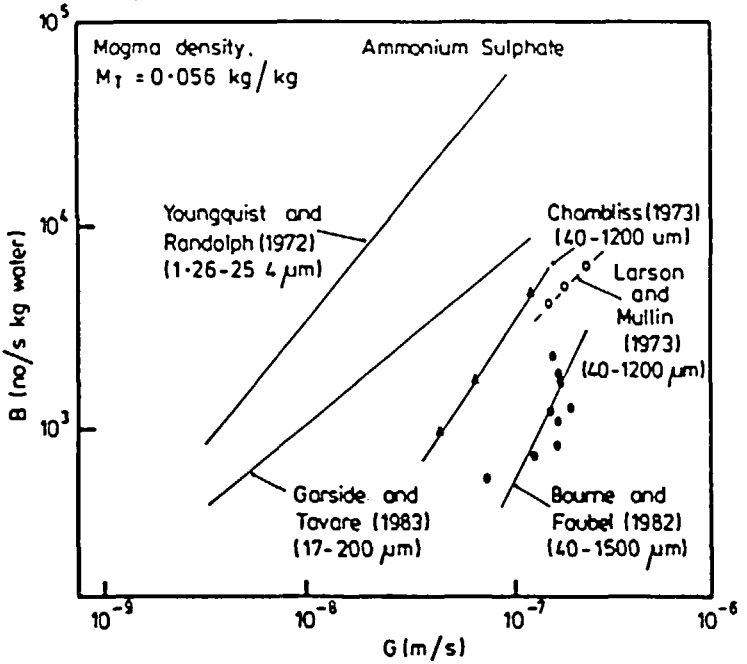

Figure 12 Comparison of relative nucleation kinetics

their determination. Thus the method of s plane analysis appears to provide a simple, accurate and seemingly reliable technique by which to extract parameter estimates from experimentally measured CSDs.

5.3 Consistency Checks

In addition to the consistency of the derived kinetic results of a system among themselves and with previous results in their totality it is in general desirable to have independent checks that should be satisfied in order to develop confidence in the estimated parameters. As mentioned before, the kinetic rates are just concepts and derived for and from the process. In the technique of parameter estimation by an iterative optimization procedure calculated

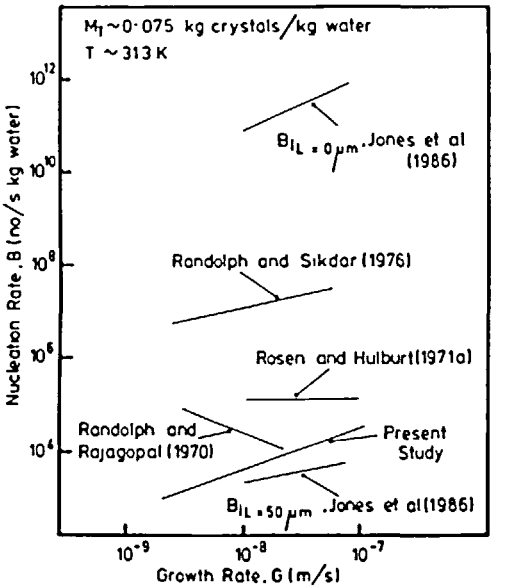

Figure 13 Comparison of relative nucleation kinetics for potassium sulphate[162]

desupersaturation curves using the best estimates evaluated from the optimization routine should closely match the experimental desupersaturation curve as can be seen, for example, in Figure 7. Slurry densities determined from the product crystal usually at the end of a run and solution concentration changes should be in good agreement indicating adequate closure of the solute balance. Prediction of growth kinetics should be normally satisfactory and mostly in good agreement with previous work (see e.g. Figure 7). The evidence given by the final product size distribution should provide a further approximate confirmation of the growth kinetic parameter estimates. Figure 14 depicts normalized differential and cumulative oversize weight distribution and the corresponding population and weight density plots for the product crystals obtained for a run, all being derived from the sieve analysis. The location of the original seed size is also shown together with the expected final size of product using the growth kinetics in Figure 8 along with the

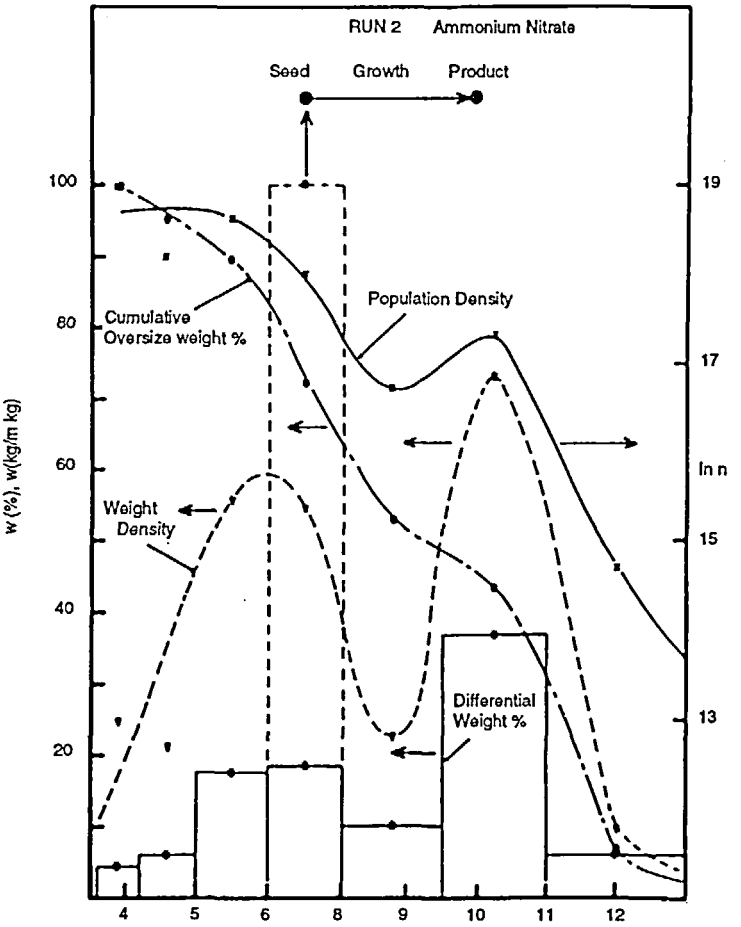

Figure 14 Typical product size analysis

experimental desupersaturation curve in Figure 7. This shows good agreement with that part of the measured product distribution and so confirms the reliability of growth rate parameters. The wider spread in actual product size distribution as compared to the narrow seed size distribution most likely arises from the phenomenon of growth rate dispersion (see sections on growth rate dispersion). The weight density plot delineates more closely than the

population density plot the two distinct peaks representing the distributions due to nuclei and seeds respectively. The effective nucleation rate determined from the desupersaturation curve is in terms of a mass deposition rate. It is rather difficult to find a suitable similar independent confirmation regarding the accuracy and precision of this rate independent of speculations concerning the mechanism or the character of nucleation process. A considerable difficulty is posed in transforming this rate to an equivalent rate on a number basis as classically used in continuous MSMPR experimentation. Kane et al.[45] assumed a population density decaying exponentially with size analogous to an MSMPR distribution at a particular time in a batch crystallizer, such a functional form could be used to define nuclei population density by matching suitable known moments of distribution. Estrin et al.[71] also used an empirical curve of an orthogonal polynomial of third degree with an exponential weighting function. Mullin and Nyvlt[84] and Nyvlt[85] have suggested several arbitrary ways of defining the nucleus size. Although it has shown that the kinetic estimates obtained from the desupersaturation curves can be used to reproduce the original desupersaturation curve in Figure 7 it is difficult to predict the population density curves with any certainty using these kinetic estimates.

Garside and Tavare[19] demonstrated with the simulated noisy experimental observations that the original size distributions can be recalculated with fair degree of confidence. The relative nucleation kinetics obtained from the method of s plane analysis using the simulated noisy Coulter counter population density data with the relative standard deviation about the true value of 20% were used to calculate the desupersaturation curve and the time evolution of the CSD. The dotted curves in Figures 4 and 5 represent the results of these calculations. The differences between the two sets of curves are comparatively small. It appears however difficult to recover the experimentally measured size distributions from the derived kinetic parameters. For example Figure 15 shows the final measured size distribution for a run and illustrates the agreement between data points obtained with the Coulter Counter and by sieve analysis. The final crystal size distribution was calculated using the kinetic correlations and experimental desupersaturation curve; this calculated distribution is also shown. Comparison of these two

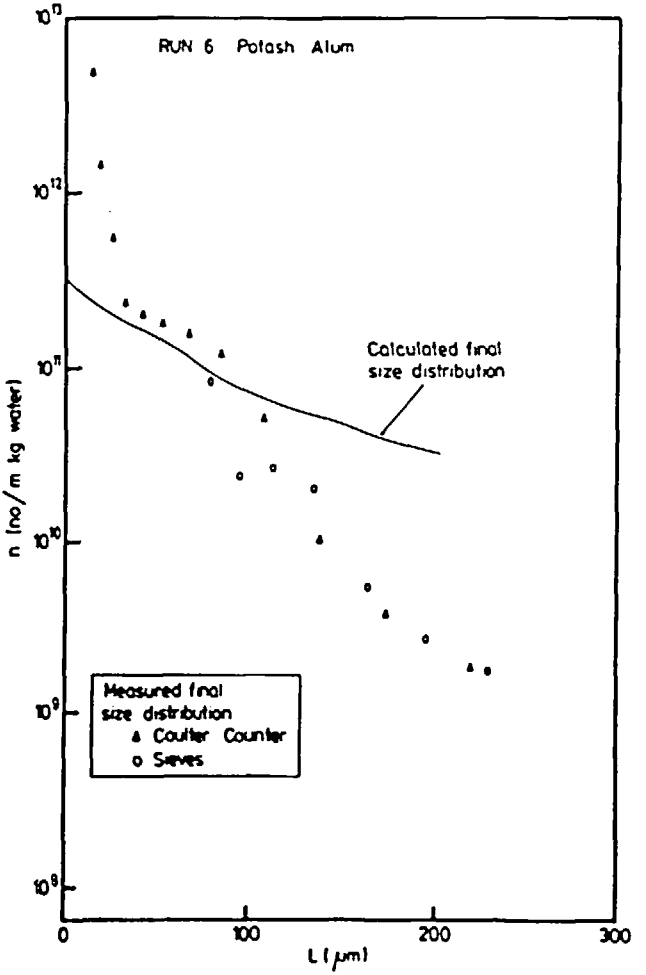

Figure 15 Comparison between measured and calculated size analysis

distributions illustrate a feature of calculations techniques based on moments. As an averaging of the distribution is involved it is frequently difficult to invert the problem and recover the data.

It is important to note that parameter estimation procedures using two different pieces of information are independent of each other and each only

uses partial information of the system. Interrelation between them to yield consistent results is difficult. A further difficulty arises from the lack of our understanding about the nucleation phenomena. It has however been demonstrated that the laboratory experiments employing a batch crystallizer provide valuable information regarding crystallization kinetics and demonstrate the relative ease with which the effect of several operating variables on growth and apparent nucleation kinetics can be correlated in a short time.

6. CHARACTERIZATION OF GROWTH RATE DISPERSION

There has been increasing recognition to the phenomenon of growth rate dispersion in analysis and characterization of the crystal growth process. The concept originated from early work on sugar crystallization[86] Since then several researchers have shown for many crystallization systems that when a group of crystals all having the same initial size are grown under globally identical external conditions of supersaturation, temperature and hydrodynamics in a batch crystallizer under negligible nucleation conditions, a stochastic variation in crystal growth rates exists and consequently a broadening in product crystal size distribution results.

Experiments of many different kinds in batch mode have shown the existence of growth rate dispersion. In their seminal work on sugar crystallization in a 5L batch crystallizer White and Wright[86] introduced a phenomenological length parameter, p, characterized from the slope of the variance of the product distribution against the mean size of the crystal population. Although there is a scatter the general trends in their results show that the magnitude of the length dispersion parameter increases with decreasing growth rate and level of impurity and is insensitive to temperature and initial seed conditions. Natalina and Treivus[87] studied the growth characteristics on numerous large (up to 20 mm) potassium dihydrogen phosphate (KDP) crystals in a growth cell by measuring size increments in two directions and observed substantial growth rate variations at all levels of supersaturation. Janse and de Jong[88] characterized growth rate and growth dispersion characteristics in a fluidized

bed crystallizer. Gabas and Laguerie[89] characterized growth rates and their dispersion for D–xylose crystals in aqueous solutions in the presence of ethanol as a co–solvent and of D–mannose as a co–solute from measured crystal size distribution by a particle size analyzer. Direct observations by photographic microscopy used by a number of investigators[90-94] clearly showed the secondary nuclei had a variety of growth rates apparently unrelated to crystal size or environment in a supersaturated solution. The behaviour of secondary nuclei has been characterized from measurements on both single crystals[90,95-97] and crystal populations[90,91,98-104] while growth of small single crystals produced by primary nucleation processes is described.[105-107] All the studies provide strong experimental evidence that very wide variations have been found for growth of nuclei produced in the microscopically visible size range either by contact secondary or primary nucleation processes. The magnitude of dispersion determined from single crystals appears generally larger than that characterized from an ensemble of crystal population,[90,108-109] although the study[22] on anhydrous sodium sulphate crystals reported smaller dispersion for single crystals.

Most of the above studies based on single crystal growth rate measurements support the view that, although the different crystals have different growth rates for given environmental conditions, a given crystal grows at a constant intrinsic rate. Perhaps the constancy of the growth rate for a given crystal may be attributed and the time scale over which the measurements are made.

Klug and Pigford[22] reported single crystal studies for the growth rate of anhydrous sodium sulphate crystals in a flow cell. Measurements of size versus time for several single crystals were observed by photomicroscopy to calculate the growth rates of individual crystals. Using this information they constructed a normalized distribution of growth rate activities. The linearity of the size versus time data for several crystals grown at identical conditions of temperature and supersaturation indicated that the individual crystals maintained constant but independent growth rate. The results also indicated the presence of the growth rate dispersion. To account for the temperature effect the growth rate data at the other temperatures was normalized at 61°C using the Arrhenius expression with activation energy of 13.7 kcal/mol. From

the spread of the measurements the growth rate dispersion effect increases with supersaturation.

The probability distribution of growth rate activities, P(g*), can be determined from single crystal growth data by recording the frequency (or number of occurrences) of specific value of g*. The value of g* can be calculated from the growth rate model as

$$G = g^* \phi(\sigma,T) \tag{56}$$

where G is the measured growth rate, g* represents a structure sensitive variable characterizing a crystal's individual growth rate activity, and $\phi(\sigma,T)$ is the driving force for crystal growth which is considered to be the same for all the crystals. The model thus assumes that a crystal's growth activity, g*, is fixed at birth and will not change with size, temperature or supersaturation. The function $\phi(\sigma,T)$ was determined by correlating the measured growth rates of the single crystals with an expression of the form

$$\phi(\sigma,T) = 1x10^{11}\sigma^2 \exp(-13700/R_gT)\tanh(0.1/\sigma) \tag{57}$$

The resulting growth rate activity distribution of single crystals computed by plotting the number of occurrence of g* vs g* is shown in Figure 16. The distribution is normalized such that the area under the curve is equal to unity. The most notable feature of the distribution is the asymmetry; greater number of crystals are found in high growth activity region. Garside and Ristic[107] also reported similar observation for the ammonium dihydrogen phosphate system. The definitions of the statistical properties used in Figure 16 are in Table 7.

In order to characterize the magnitude of the growth dispersion phenomenon Janse and de Jong[110] assumed that the growth rate is an independent property of a crystal as each crystal grows at its own constant intrinsic growth rate throughout the life span in an environment and defined a two dimensional modified population density function characterized by two variables viz. crystal size and growth rate. Such an approach should add an additional dimension to the number conservation equation and require an additional

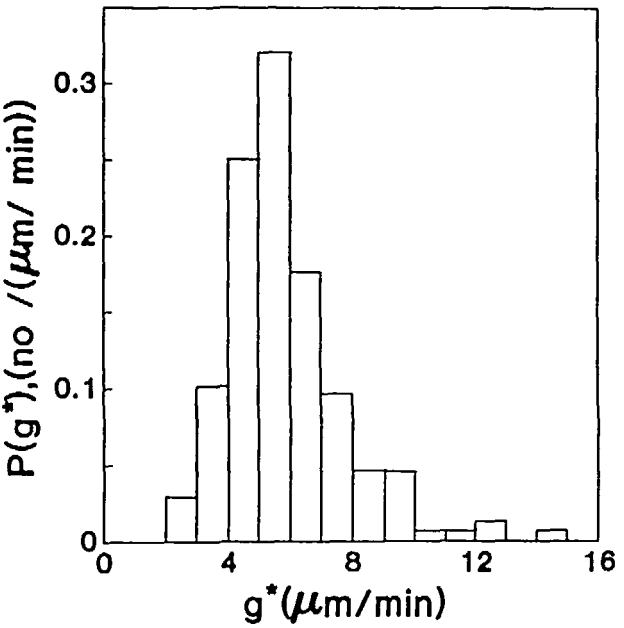

Figure 16 Distribution of growth rate activities, P(g*), of anhydrous sodium sulphate crystals as determined from single crystal growth studies
Total number of crystals measured =209
Range of crystal sizes $20 - 400\mu m$
Results of statistical analysis
Average growth rate activity = $\langle P(g^*)\rangle_1 = 5.5\mu m$
Second moment = $\langle P(g^*)\rangle_2 = 36.1\ (\mu m/min)^2$
Third moment = $\langle P(g^*)\rangle_3 = 253\ (\mu m/min)^3$
Standard deviation = SD = 1.8 (μm/min)
Coefficient of variation = CV = 32 %
Skewness = K = 1.4

constraint to define the system. Usually the growth rate dispersion in the form of a statistical distribution (e.g. by gamma distribution) has been arbitrarily used[110-111] Such modelling may make the characterization of growth rate dispersion difficult from the response of the system. The growth

Table 7 Statistical properties of the distribution (Figure 16)

$$\int_0^\infty P(g^*)dg^* = 1$$

$$\langle P(g^*)\rangle_j = \text{j th moment} = \int_0^\infty g^{*j}P(g^*)dg^*$$

$$\bar{g}^* = \text{mean} = \int_0^\infty g^*P(g^*)dg^*$$

$$\zeta_j = \text{j th central moment} = \int_0^\infty (g^*-\bar{g}^*)^jP(g^*)dg^*$$

$$\zeta_2 = \langle P(g^*)\rangle_2 - \langle P(g^*)\rangle_1^2$$

$$\zeta_3 = \langle P(g^*)\rangle_3 - 3\langle P(g^*)\rangle_1\langle P(g^*)\rangle_2 + 2\langle P(g^*)\rangle_1^3$$

$$\text{standard deviation SD} = \zeta_2^{0.5}$$

$$\text{coefficient of variation CV} = SD/\bar{g}^*$$

$$\text{skewness} = K = \zeta_3/SD^3$$

rate of a crystal assumed as a property is usually determined from the gradient of the crystal size–time variation. Randolph and White[112] in their modelling of such growth behaviour pointed out the close analogy between growth rate dispersion and axial dispersion in near plug flow reactors. The mixing processes are statistical in nature and represented by the diffusion type equation in the dispersion models which provide a macroscopic description of a chemical reactor to quantify the backmixing characteristics. The dispersion effects in crystallization due to random fluctuations in growth rate and flow can be described analogously by the macroscopic population balance for an isothermal batch crystallizer as

$$\frac{\partial n}{\partial t} + \bar{G}\frac{\partial n}{\partial L} = D_G\frac{\partial^2 n}{\partial L^2} \tag{58}$$

The growth dispersion model represented by equation (58) takes the form of a one dimensional second order partial differential equation and is characterized by two model parameters, $\bar{G}$ the average linear growth rate and D_G the effective growth rate diffusivity. With the assumption of constant supersaturation throughout the run and size independent growth the average

growth rate may be a time and space average value. A dispersion coefficient will in general be a function of both system properties and flow situations and be non–isotropic in character. However, the effective growth rate diffusivity used in equation (58) is assumed to be size and position independent within the system and will be assumed to characterize uniquely the degree of non–ideality present as a consequence of random fluctuation in growth rates. Selection of the boundary conditions to describe the physical situation mathematically is also important. Several sets of boundary conditions have been suggested to describe the dispersion model in chemical reactors![13] In general, a minimum of two boundary conditions or constraints is necessary although an unconstrained general solution is sometimes possible.

The first condition is for the flux entrance (by an initial impulse in the present case) and may be represented as

$$n(L,0) = f(L) \tag{59}$$

where f(L) is the initial seed CSD. For the specific case where the crystallizer is seeded initially with narrowly sized crystals obtained, for example, from the material retained between two adjacent sieve sizes, differing by ΔL_0 and having mean size L_0, the seed population density will be assumed to have a point value of n_0 at L_0 determined by

$$n_0 = \frac{W_0}{\rho_c k_v L_0^3 \Delta L_0 S_0} \tag{60}$$

In this case f(L) will be

$$f(L) = n_0 \Delta L_0 \delta(L - L_0) \tag{61}$$

The form of function f(L) may also be derived by measurement of the initial crystal size distribution. Its specific form is unimportant in the most of the techniques discussed subsequently.

The second condition may be derived from the assumption of a semi–infinite continuum for the population density function which for infinite size must

Table 8: Methods available to determine parameters of the dispersion model (equation 58) by pulse stimulus response analysis

Time domain
1.Method of moments
(a)with respect to characteristic length
(b)with respect to time
2.Characteristic points
3.Optimization methods[114,115]
Laplace transform domain
1.Method of moments in time domain
2.Four methods of Michelsen and Ostergaard[116]
3.Method of Abbi and Gunn[115]
4.Numerical integration or inversion of Laplace transform[115]
5.Optimization methods[117]
Frequency domain
1.Method of moments from frequency response
2.Method of Abbi and Gunn[115]
3.Method of Rosen and Winsche[118]
4.Optimization methods[114,119]

tend to zero, i.e.,

$$n(\infty,t) = 0 \tag{62}$$

6.1 Parameter Characterization

A number of methods can be used to characterize the parameters of the dispersion model (equation 58) from the pulse stimulus response as has been used in chemical reactors. These are listed in Table 8. Some of the available

methods will be discussed and in some cases the applications to the specific experimental data illustrated.

6.1.1 Time domain methods

6.1.1.1 Method of Moments

The use of moments in system response analysis for parameter estimation in linear models involves matching moments of the system model output to like moments of experimental data. The kth moments of the population density distribution about the origin obtained by moment transformation with respect to size can be defined as

$$m_k = \int_0^\infty nL^k dL \tag{63}$$

Randolph and White[112] employed such a moment transformation technique in modelling size dispersion effects in crystallizer configurations. Tavare and Garside[108] used first and second central moments of the observed population density distribution of the product from a fluidized bed crystallizer that had been seeded with a narrow size distribution. The model parameters were characterized as

$$\bar{G} = \frac{\Delta L}{\tau} \tag{64}$$

and

$$D_G = \frac{\Delta \sigma_L^2}{2\tau} \tag{65}$$

where ΔL and $\Delta \sigma_L^2$ are the differences in initial and final average size and variance respectively over a batch time τ. This is an example of a representation type of problem where the input functions are known. Following the treatment suggested by Aris[120] the same analysis can be extended to an identification type problem where the form of input forcing function need not be known. In this case the application of equations (64–65)

requires measurements of $\bar{L}$ and σ_L^2 at two separate times differing by τ so as to evaluate ΔL and $\Delta\sigma_L^2$. Thus both single and two shot methods can be used. In single shot methods the response at any one time after the impulse is used and the mean and variance relative to the initial impulse evaluated from the first and second moments. In two shot method the responses at two different times after the impulse are determined and the corresponding differences in mean and variance of the distribution calculated. Average growth rates and their diffusivities are then evaluated by equations (64–65).

If the following dimensionless variables are defined as

$$x = L/\bar{G}\tau \qquad T = t/\tau \qquad y = n\bar{G}/B$$

the growth dispersion model (equation 58) can be rewritten in terms of dimensionless variables as

$$\frac{\partial y}{\partial T} + \frac{\partial y}{\partial x} = \frac{1}{Pe}\frac{\partial^2 y}{\partial x^2} \tag{66}$$

with boundary conditions for flux at zero size

$$y(T,0) = f(T) \tag{67}$$

and for initial CSD

$$y(0,x) = 0 \tag{68}$$

In order to have finite values for all y and remain bounded

$$y(0,\infty) = 0 \tag{69}$$

Taking the Laplace transform of equation (66) with respect to T

$$\left[\frac{1}{Pe} D^2 - D - p\right]\bar{y}(p,x) = -y(0,x) \tag{70}$$

Solving for $\bar{y}(p,x)$ and using the boundary conditions, we get

$$\bar{y}(p,x) = \bar{f}(p)\exp[\{\frac{Pe}{2}(1-\sqrt{1+(4p/Pe)})\}x] \tag{71}$$

Now assuming that the moments of f(T) exist i.e. flux at zero is finite and function of time and $\bar{f}(p)$ and also $\bar{y}(p,x)$ are analytic at origin the kth moment of y(T,x) with respect to T can be defined as

$$U_k = \int_0^\infty y(T,x)T^k dT = (-1)^k \frac{d^n \bar{y}(p,x)}{dp^n}\Big|_{p=0} \tag{72}$$

Using equation (72) the moments can be evaluated as

$$U_0(x) = \bar{y}(0,x) = \bar{f}(0) = U_{00} \tag{73}$$

$$U_1(x) = -\dot{\bar{f}}(0) + \bar{f}(0)x \tag{74}$$

Assuming $\bar{f}(0) = U_{00} = U_0(x) = 1$

$$U_1(x) = (U_1(x)-U_1(0))/U_0(x) = x \tag{75}$$

$$U_2(x) = \ddot{\bar{f}}(0)-2x\dot{\bar{f}}(0)+x^2\bar{f}(0)+(2x/Pe)\bar{f}(0) \tag{76}$$

$$= \ddot{\bar{f}}(0)+x^2+2x/Pe \tag{77}$$

Here we assume $U_{10} = -\dot{\bar{f}}(0) = 0$ and $U_0 = \bar{f}(0) = 1$.
Thus the changes in the mean and variance for the growth dispersion model (equation 58) are

$$\mu = U_1(x) = x$$

and

$$\sigma^2-\sigma_0^2 = U_2(x)-U_1(x)^2-\sigma_0^2 = \ddot{\bar{f}}(0)+x^2+(2x/Pe)-x^2-\ddot{\bar{f}}(0)$$

$$= 2x/Pe \tag{78}$$

Table 9: Growth rates and growth rate diffusivities calculated from moment transformation with respect to size in the time domain for potash alum for Δc = 0.0055kg hydrate/kg solution at T =303 K.

Δt, s	$\bar{L}$, μm	$\bar{G}$, μm/s	D_G, $\mu m^2/s$
0 –150	16.6–19.7	0.020	0.09
0 –285	16.6–23.2	0.022	0.08
150–285	19.7–23.2	0.025	0.08

Although the original experiments were used by Garside and Jancic[121] to characterize the growth kinetics of small (<~40 μm size) crystals the same results can be used to characterize the growth and growth dispersion parameters. The results in their Figure 3 shows results obtained from an experiment performed in a 250 mL isothermal batch crystallizer seeded with small potash alum crystals obtained either from an operating continuous crystallizer or from a careful milling operation. Constant supersaturation was maintained. The results of growth rate and growth rate diffusivity are reported in Table 9. The calculated values of $\bar{G}$ and D_G appear consistent between the two calculation methods.

The use of lower (up to second order) moments is most convenient and sufficiently accurate for the interpretation of response data because of the smoothing effect of the integration process. As, in most cases, the product CSD at longer time tends to a normal distribution and uncertainties in measurement exist towards the tail of the distribution, use of higher order moments is not reliable. Application of this method assumes that the mathematical description is exact, provides no direct check of model validity for the current system and is limited in model discrimination when several alternative descriptions are available.

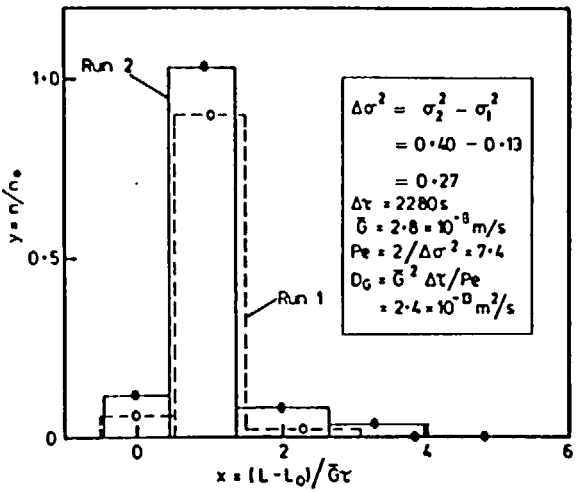

Figure 17 Evaluation of Peclet number and growth rate diffusivities

Tavare and Garside[122] suggested a two shot method to characterize Peclet number for crystal growth ($Pe = D_G/\bar{G}^2\tau$) using the difference between dimensionless variance. They used the data from two experiments conducted in a differential mode under otherwise identical conditions, differing only in batch time for crystallization of potassium sulphate crystals in a fluidized bed crystallizer. Dimensionless population density plot on linear scale for these two runs is shown in Figure 17. The calculated Peclet number in this case (Pe = 7.4) is comparable with those values (Pe = 15.4 and 4.9) calculated by the method of moments used on single run measurements.

6.1.1.2 Characteristic points

Aris[123] showed that the response of the most general dispersion model with its large number of parameters also approaches a normal distribution for larger times. Certain characteristic points of this distribution such as the maximum and points of inflection can be used in evaluating approximate values of the

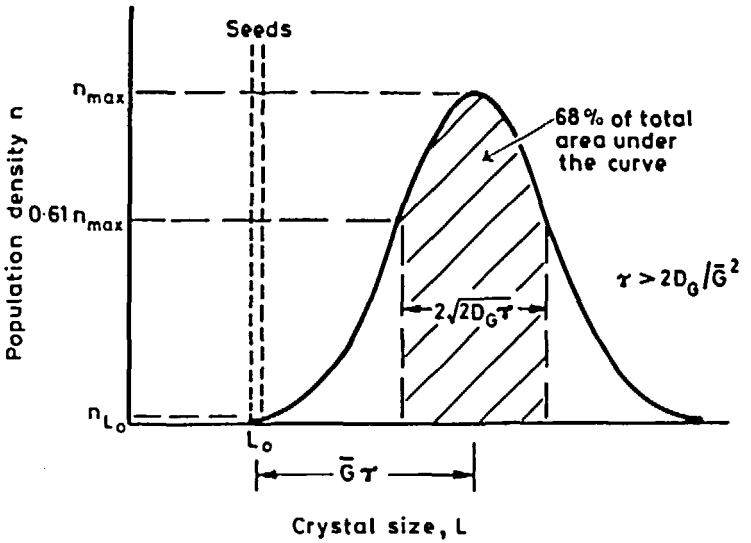

Figure 18 Use of characteristic points: Response from a spike impulse of a population B_0/G at L_0

$$n(t,L) = \frac{B_0}{2\sqrt{\pi D_G \tau}} \exp\left[-\frac{(L - L_0 - \bar{G}t)^2}{4D_G\tau}\right]$$

$$n_{max} = \frac{B_0}{2\sqrt{\pi D_G \tau}}$$

$$n_{L_0} = \frac{B_0}{2\sqrt{\pi D_G \tau}} \exp\left[-\frac{\bar{G}^2\tau}{4D_G}\right]$$

parameters as illustrated in Figure 18. Growth rate diffusivity determined from the width at the inflection points of the experimental population density measured at the end of the growth run for potash alum in a small batch crystallizer is 0.07 $\mu m^2/s$. This is in fair agreement with results obtained from the method of moments (Table 9). Such determinations only provide order of magnitude estimates as they use a very limited amount of information and characteristic points are often difficult to define with precision.

6.1.2 Laplace Transform Domain Methods

It is often advantageous to estimate model parameters in the Laplace transform rather than the time domain. The transfer function for any stable linear one dimensional system can be evaluated from the experimental response using the imperfect pulse method by numerical integration of the transient response to an arbitrary forcing function measured at two points (as in identification problems). The experimentally determined transient response can be converted into moments of the form

$$M^{n,p} = \int_0^\infty n(t,L)\exp(-pt)t^n dt = (-1)^n \frac{d^n \bar{n}(p,L)}{dt^n} \tag{79}$$

where

$$\bar{n} = \int_0^\infty n(t,L)\exp(-pt)dt \tag{80}$$

The Laplace transform and its derivatives are related to the system transfer functions, F, through the relations

$$F = \frac{\bar{n}(p,L_2)}{\bar{n}(p,L_1)} \tag{81}$$

$$\frac{\dot{F}}{F} = \left[\frac{\dot{\bar{n}}(p,L)}{\bar{n}(p,L)}\right]\Bigg|_{L_1}^{L_2} \tag{82}$$

$$\frac{\ddot{F}}{F} - \left[\frac{\dot{F}}{F}\right]^2 = \left[\frac{\ddot{\bar{n}}(p,L)}{\bar{n}(p,L)} - \left[\frac{\dot{\bar{n}}(p,L)}{\bar{n}(p,L)}\right]^2\right]\Bigg|_{L_1}^{L_2} \tag{83}$$

or in general

$$\frac{d^n(\dot{F}/F)}{dp^n} = \left[\frac{d^n}{dp^n}\left[\frac{\dot{\bar{n}}(p,L)}{\bar{n}(p,L)}\right]\right]\Bigg|_{L_1}^{L_2}. \tag{84}$$

The right hand sides of these equations can be evaluated by computation of moments, $M^{n,p}$, so that F and its derivatives may be determined for an arbitrary number of p values. The values of the transfer function and/or its derivatives may then be used to check the validity of the system model and evaluate the parameters within the model. The system transfer function for the growth dispersion model (equation 58) obtained by taking the Laplace transform under the conditions represented by equations (59–62) can be derived as

$$F = \exp\left[\frac{\bar{G}\Delta L}{2D_G}(1-q)\right] \tag{85}$$

where

$$q = \sqrt{\left[1+(4D_G p/\bar{G}^2)\right]} \tag{86}$$

and ΔL is the difference between L_2 and L_1, the two sizes at which the population density as a function of time will be determined. The logarithmic transfer function, its derivatives, moments and the model parameters are related by

$$U_0 = \ln F = [\ln M^{0,p}]\Big|_{L_1}^{L_2} = \left[\frac{\bar{G}\Delta L}{2D_G}\right](1-q) \tag{87}$$

$$U_1 = \frac{\dot{F}}{F} = \left[\frac{M^{1,p}}{M^{0,p}}\right]\Big|_{L_1}^{L_2} = \frac{\Delta L}{\bar{G}q} \tag{88}$$

and

$$U_2 = \frac{\ddot{F}}{F} - \left(\frac{\dot{F}}{F}\right)^2 = \left[\frac{M^{2,p}}{M^{0,p}} - \left(\frac{M^{1,p}}{M^{0,p}}\right)^2\right]\Bigg|_{L_1}^{L_2}$$
$$= \frac{2D_G\Delta L}{\bar{G}^3 q^3} \tag{89}$$

Parameter evaluation for a model containing r parameters requires calculation of at least r moments. It will normally be advantageous to compute a large

number of moments and evaluate the parameters by statistical analysis because the validity of the system model can thereby be assessed.

6.1.2.1 Method of Moments in Time Domain

Moment transformation of equation (58) with respect to time can also be carried out in a similar way to that used for size. However these moments can be derived easily from the Laplace transform domain by using the evaluations of derivatives at $p = 0$ in the general equation (equation 84). Thus

$$U_1\Big|_{p=0} = \left[\frac{M^{1,0}}{M^{0,0}}\right]\Bigg|_{L_1}^{L_2} = \frac{\Delta L}{\bar{G}} \tag{90}$$

$$U_2\Big|_{p=0} = \left[\frac{M^{2,0}}{M^{0,0}} - \left[\frac{M^{1,0}}{M^{0,0}}\right]^2\right]\Bigg|_{L_1}^{L_2} = \frac{2D_G\Delta L}{\bar{G}^3} \tag{91}$$

Equations (90–91) can be used to determine $\bar{G}$ and D_G from experimental data of population density as a function of time at two sizes ΔL apart.

6.1.2.2 Methods of Michelsen and Ostergaard[116]

These are modifications of the moments method in which the moments of the response are modified by a damped exponential weighting factor to minimize error magnifications towards the tails of the response. Four methods are suggested:

(i)If the moments $M^{0,P}$ and $M^{1,P}$ are available simultaneously for any p the model parameters can be obtained from

$$\frac{\Delta L}{\bar{G}} = -\frac{U_0 U_1}{U_0 + 2pU_1} \tag{92}$$

$$\frac{\bar{G}\Delta L}{D_G} = \frac{U_0(U_0+2pU_1)}{U_0+pU_1} \tag{93}$$

these equations being derived from equations (87–88).

(ii)If the moments $M^{0,p}$, $M^{1,p}$ and $M^{2,p}$ are calculated for any p simultaneously from the response the model parameters may be deduced from

$$\frac{\Delta L}{\bar{G}} = U_1\left[1-2p\frac{U_2}{U_1}\right]^{-\frac{1}{2}} \tag{94}$$

$$\frac{\bar{G}\Delta L}{D_G} = 2\frac{U_1^2}{U_2}\left[1-2p\frac{U_2}{U_1}\right]^{\frac{1}{2}} \tag{95}$$

These results are formulated from relations (88–89).

(iii)Equation (87) can be modified to

$$-\frac{1}{U_0} = \frac{\Delta L p}{\bar{G}\ U_0^2} - \frac{D_G}{\bar{G}\Delta L} \tag{96}$$

Thus if the moment $M^{0,p}$ is evaluated for a number of p values a plot of $-1/U_0$ *versus* p/U_0^2 gives straight line of slope $\Delta L/\bar{G}$ and intercept $-D_G/\bar{G}\Delta L$ on the ordinate.

(iv)Equation (88) may be rewritten as

$$\frac{1}{U_1^2} = \frac{4D_G p}{\Delta L^2} + \frac{\bar{G}^2}{\Delta L^2} \tag{97}$$

If the moments $M^{0,p}$ and $M^{1,p}$ are available for a number of values of p a plot of $1/U_1^2$ against p thus yields a straight line of slope $4D_G/\Delta L^2$ and intercept $\bar{G}^2/\Delta L^2$.

6.1.2.3 Method of Abbi and Gunn[115]

These authors expanded the square root term in the expression for q (equation 86) using the binomial theorem. When used with equation (87) this gives

$$U_0 = \frac{\bar{G}\Delta L}{2D_G}\left[1 - \left[1 + \frac{2D_G p}{\bar{G}^2} - \frac{2D_G{}^2 p^2}{\bar{G}^4} + O(p^3)\right]\right] \tag{98}$$

Using only the first three terms in the expansion this can be written

$$\frac{1}{p}U_0 = \frac{D_G \Delta L}{\bar{G}^3}p - \frac{\Delta L}{\bar{G}} \tag{99}$$

Because of the limitation of the accuracy of this approximation equation (99) will only be an accurate representation provided $0<4D_G p/\bar{G}^2<0.2$–0.4 so establishing an upper bound to the values of p. Given this proviso equation (99) represents a straight line with intercept $-\Delta L/\bar{G}$ and gradient $D_G \Delta L/\bar{G}^3$.

One of the obvious advantages in using the Laplace domain methods is that the sensitivity to experimental errors in the determination of the transient response is greatly reduced provided suitable values of the Laplace transform variable, p, are used. If the chosen value of p is too small the tail will be heavily weighted whereas if it is too high, too much emphasis will be given to the front portion of the response. In either case a poor estimate of weighted moments will result. Michelsen and Ostergaard[116] treated the problem of finding the optimal p values by using the noise sensitivity function and suggested that the optimal values of $p\bar{t}$ for the first and third of their methods is in the range 0.5–2 while for the second and fourth methods it is close to unity. Anderson and White[124] empirically proposed that the optimum weight factor for use with the kth moment in an identification type problem can be defined as

$$p_{opt} = 2(k_{av}+1)/(\bar{t}_1+\bar{t}_2-\Delta t) \tag{100}$$

where $\bar{t}_1$ and $\bar{t}_2$ are the mean times of the distribution at sizes L_1 and L_2 respectively, $\Delta t = \bar{t}_2 - \bar{t}_1$ and k_{avg} is the order of the moments used to estimate these parameters (i. e. $k_{avg} = 0.5k_{max}$). Hopkins et al[125] pointed out that the use of low $p\bar{t}$ values provide no information on model discrimination as most of the models will have more or less the same response in dispersion characterization and recommended that, to have consistent results, the suitable range of $p\bar{t}$ for flow through packed beds is 2–5. However, Abbi and Gunn[115] argued that, for a given model, there is no particular merit in this suggestion as the relative weighting of the points within the range, particularly towards the lower end, is influential.

The cross plots of the published experimental population density – size data at various sample times are shown in Figure 3 of Tavare and Garside[109] and represent the variation of population density with time at two different values of size. The values of $\bar{G}$ and D_G obtained from the data of Purves and Larson[99] in their Figure 3 using several methods are reported in Table 10. Derived values of $\bar{G}$ and D_G from the Laplace transform domain methods are very sensitive to the range of p. In the first of the methods suggested by Michelsen and Ostergaard[116] the results are evaluated from the moments up to first order whereas the second utilizes the second order moment variant thus the first method usually resulting a better estimates in all cases. In general, inaccuracies in evaluating higher order moments will be more severe than for the first order moments so that methods using lower moment variants are likely to produce better performance. The optimal range of p suggested by Michelsen and Ostergaard[116] ($0.5<p\bar{t}<2$) requiring an elaborate calculation procedure in addition to knowledge of the noise function seems precise. The suggestions of Anderson and White[124] and Abbi and Gunn[115] involve simplified calculations and yet provide fairly similar estimates to those obtained by the procedure of Michelsen and Ostergaard[116] In formulating the linear regression to estimate the parameters using the remaining methods (equations 96,97,99), the limits on p values (i.e. $p\bar{t}$ up to 3) suggested by Michelsen and Ostergaard[116] on the basis of their analysis seem appropriate for the linear regression. The constraints suggested by Abbi and Gunn[115] for accurate representation of the square root term in equation (85) by the binomial

Table 10: Growth rates and diffusivities estimated using various methods for potassium nitrate[99]

Methods	eqs used	$\bar{G}$, μm/s	D_G, $\mu m^2/s$
1. Time domain			
(a)moments	64,65	~0.15	~1.2
(b)characteristic points			0.6
2. Laplace transform domain			
(a)moments	90,91	0.53	0.78
(b)Michelsen and Ostergaard[116]			
(i)	92,93	0.54	0.68
(ii)	94,95	0.52	0.79
(iii)	96	0.55	0.38
(iv)	97	0.51	1.19
(c)Abbi and Gunn[115]	99	0.54	0.55
3. Frequency domain			
(a)moments from the frequency response	107,108		
(b)Abbi and Gunn[115]	106,112	0.55	0.03
(c)Rosen and Winsche[118]		0.55	0.04

theorem also provides a satisfactory choice of the maximum allowable p values (i.e. $p_{max} = 0.1\bar{G}^2/D_G$).

Although the correlation coefficient r of $(-1/U_0)$ upon (p/U_0^2) in the linear regression was very close to unity for the chosen range of p for the system, the value of D_G had to be calculated from very small values of the intercept. The correlation representing equations (97,99) are reasonably good for the system

although significant curvature was apparent in some cases. Such curvature might arise either because the dispersion model did not adequately represent the data or because the quality of the experimental data itself was unsatisfactory. Nevertheless, the representation of the results was sufficiently good to encourage further work along these lines.

6.1.3 Frequency Domain Methods

Frequency response testing is another classic technique used for parameter estimation and design in linear control systems. The frequency response transfer function of a stable linear one dimensional system to an impulse forcing function is simply the Fourier transform of the time domain response (or the Laplace transform with $p = i\omega$ in equation 80); thus

$$\bar{n}(i\omega,L) = \int_0^\infty n(t,L)\exp(-i\omega t)dt \tag{101}$$

or a complex sum of Fourier sine or cosine transformations

$$\bar{n}(i\omega,L) = \int_0^\infty n(t,L)\cos(\omega t)dt - i\int_0^\infty n(t,L)\sin(\omega t)dt \tag{102}$$

The frequency response transfer function can be related to moments by using the series expansion for the sine and cosine terms in equation (102) and the definition of non–central moments of the population density with respect to time as

$$\bar{n}(i\omega,L) = \mu_0 - \mu_2\frac{\omega^2}{2!} + \mu_4\frac{\omega^4}{4!} - .... + i\left[-\mu_1\frac{\omega}{1!} + \mu_3\frac{\omega^3}{3!} - \mu_5\frac{\omega^5}{5!} + ...\right] \tag{103}$$

The magnitude and phase angle of the frequency response transfer function can be directly related in terms of central moments by comparing with the basic definition of cumulants of a density function as

$$\ln|\bar{n}(i\omega,L)| = \nu_0 - \nu_2\frac{\omega^2}{2!} + ... \tag{104}$$

and

$$\angle \bar{n}(i\omega,L) = -\nu_1\omega + \nu_3\frac{\omega^3}{3!} - .... \tag{105}$$

Examination of equation (104) reveals that the modulus of the transfer function $|\bar{n}(i\omega,L)|$, i.e. the magnitude ratio, is expanded in terms of even central moments, the first two being the gain and the variance of the system. The argument $\angle \bar{n}(i\omega,L)$ or the phase shift given by equation (105) is expanded in terms of odd central moments, the first two being the mean and the skewness of the distribution. Since the impulse response of many systems under test tends towards a displaced normal distribution of negligible skewness, the phase shift becomes that of a pure time delay (as in plug flow configurations), i.e.

$$\angle \bar{n}(i\omega,L) \approx -\nu_1\omega \tag{106}$$

Clearly, if $|\bar{n}(i\omega,L)|$ and $\angle \bar{n}(i\omega,L)$ have been obtained by pulse testing and conversion to the frequency domain, the moments estimated by curve fitting to $|\bar{n}(i\omega,L)|$ and $\angle \bar{n}(i\omega,L)$ can be no more accurate than those that would be obtained by direct moment analysis of the time domain data.

6.1.3.1 Method of Moments Derived from Frequency Response

By analogy with the Laplace domain the relationship between frequency response and the central moments with respect to time can be established as

$$\mu_1 = \lim_{\omega \to 0}\left[\frac{d\angle F}{d\omega}\right] = \frac{\Delta L}{\bar{G}} \tag{107}$$

$$\mu_2 = -\lim_{\omega \to 0}\left[\frac{d^2 \ln|F|}{d\omega^2}\right] = \frac{2D_G\,\Delta L}{\bar{G}^3} \tag{108}$$

where

$F = \bar{n}(i\omega,L_2)/\bar{n}(i\omega,L_1)$, $\angle F$ = absolute phase shift and $|F|$ = magnitude ratio.

From the practical point of view computation of impulse response moments by differentiation of an experimental frequency response in the region of zero frequency is however likely to be even more prone to error than direct estimation of moments.

6.1.3.2 Method by Abbi and Gunn[115]

The amplitude ratio, AR, of the frequency response transfer function can be determined from the experimental response of the population density as a function of time at two sizes from equation (81) using

$$AR = |F| = \left[\frac{(C_2C_1+S_2S_1)^2 + (S_2C_1-C_2S_1)^2}{(C_1^2+S_1^2)^2}\right]^{0.5} \tag{109}$$

where C_i and S_i are the cosine and sine Fourier transforms of the population density at size L_i. The experimental AR has to be determined by numerical integration of the time domain transient response to an arbitrary impulse forcing function measured at two sizes. The argument or the absolute phase shift can be defined as

$$PS = \angle F = \frac{S_2C_1-S_1C_2}{C_2C_1+S_2S_1} \tag{110}$$

The model amplitude ratio, AR, derived from equation (85) after substituting $p = i\omega$ is

$$\ln AR = \frac{\bar{G}\Delta L}{2D_G}\left\{1 - \left[\frac{1}{2} + \frac{1}{2}\left[1 + \frac{D_G^2\,\omega^2}{\bar{G}^4}\right]^{0.5}\right]^{0.5}\right\} \tag{111}$$

For relatively small ω the right hand side of equation (111) may be expanded by the binomial theorem giving

$$\ln AR = -\frac{D_G\,\Delta L}{\bar{G}^3}\omega^2 + O(\omega^4) \tag{112}$$

which is identical to equation (104) with $\nu_0 = 0$.

A plot of ln AR against ω^2 will therefore give a straight line through the origin, with slope $-D_G\Delta L/\bar{G}^3$ for a range of small values of ω. Similarly, a plot of the phase shift, PS, against ω will yield a straight line through the origin with a gradient $\Delta L/\bar{G}$.

6.1.3.3 Method by Rosen and Winsche[118]

These authors suggested that a plot of the ratio $[\ln|F|/\angle F]$, i. e. (ln AR)/PS against ω, will be linear with $-(\nu_2/2!\nu_1)$ when $(\nu_4-\nu_2\nu_3)$ is negligible over the range of ω encountered. Such an analysis requires a larger mean residence time for reliable results. The slope of the plot which equals $-D_G/\bar{G}^2$ in the present case can then be used to determine the growth diffusivities, if the growth dispersion model is applicable.

As frequency domain techniques are similar to those in the Laplace domain a suitable range of ω is also essential while deriving the parameters from the transients response. Jeffreson[119] suggested the parameters fitting should be carried out over the range of frequencies decided by $0<\omega\bar{t}<1$ as the higher order terms in equations (104,105) will make a negligible contribution to summation over the smaller frequency range. If such a range is used the frequency response will yield identical parameters to the time domain moment analysis, provided the experimental data actually fits the proposed model, so giving evidence of model validity. It was also pointed out that the suitable time interval for numerical integration should be less than 10% of the minimum half period. Clements and Schenelle[126] and Johnson et al.[127] suggested that the maximum allowable theoretical frequency range will be decided by the normalized frequency content. If this approaches the order of magnitude of experimental error the reliability of the frequency domain estimates is hampered. For systems whose response times are larger the normalized frequency content will always be greater than the experimental error for all ω and will not provide any suitable range for an idealized input forcing function.

The final results of regression analysis of equations (109, 110, 112) using the appropriate range of ω as suggested by Jeffreson[119] (i.e. $0<\omega\bar{t}<1$) in the frequency domain methods for the data set of Purves and Larson[99] are included in Table 10. The amplitude ratio for this data set is little over unity in the vicinity of $\omega \rightarrow 0$ so the gradients yielded negative values giving unrealistic parameters.

In general the techniques discussed in Table 10 are simple and illustrate an important point, viz., that it is normally necessary to try several approaches to analyze data from an experimental test. The parameter technique which will produce the most consistent parameter estimates will depend on the quality of the data and the form of the model. The techniques based on the Laplace transform and frequency domain are less sensitive to experimental errors and the numerical techniques used for the integral evaluation. The Laplace domain methods can be used to estimate the dispersion parameters from pulse response analysis because of simplicity, rapidity and reliability.

The several methods used in the determination of crystal growth dispersion characteristics by dynamic response analysis in crystallization systems can conveniently be grouped into three classes; utilization of analytical relations between the process coefficients and certain integrals of the response such as the method of moments, examination of the functional dependence of the coefficients upon parameters involved in the integral such as p or ω in addition to the analytical relations and minimization of the variance of the experimental measurements about a theoretical curve, the use of first two classes being demonstrated in this study. Third class can also be considered for the specific case by choosing the model parameters, i. e. $\bar{G}$ and D_G, associated with the minimum variance derived through optimization procedures. The variance may be calculated in time by numerical integration of the partial differential equation or by inverting the process transfer functions in the Laplace transform or the frequency domains. Although the methods using optimization procedures are potentially the most accurate and precise they demand more computation time and complexity when iterative techniques have to be adopted.

6.1.4 Growth Rate Activity Distribution

The growth rate model suggested by Klug and Pigford[22] in terms of the growth rate activity and the driving force (equations 56–57) can be used to derive growth and dispersion parameters in terms of moments of the unknown growth rate probability distributions from a seeded or unseeded batch crystallizer with time–varying supersaturation, using the stochastic model. In addition to the conventional population density function, n(t,L), representing the entire population of crystals in the crystallizer let $\bar{n}(t,L;g^*)$ be one of subpopulations, in which every crystal has the same value of the growth rate activity, g^* then it follows that

$$n(t,L) = \int_0^\infty \bar{n}(t,L;g^*)dg^* \tag{113}$$

The population balance equation for a subpopulation of crystals with growth rate activity, g^*, in a batch crystallizer as

$$\frac{\partial \bar{n}(t,L;g^*)}{\partial t} + g^*\phi(\sigma,T)\frac{\partial \bar{n}(t,L;g^*)}{\partial L} = 0 \tag{114}$$

By defining the new transformation variables as

$$\Theta = \int_0^t \phi(\sigma,T) \qquad \text{or } \frac{d\Theta}{dt} = \phi(\sigma,T) \tag{115}$$

equation(114) becomes

$$\frac{\partial \bar{n}(\Theta,L;g^*)}{\partial \Theta} + g^*\frac{\partial \bar{n}(\Theta,L;g^*)}{\partial L} = 0 \tag{116}$$

The relation between Θ and the sampling time, t can be determined from equation(115) by numerical evaluation of the integral and the population density, $n(\Theta,L)$ can be determined from the size analysis of the suspension samples. The relationship between the time dependent moments of the crystal size distribution and the moments of unknown growth rate activity distribution, $P(g^*)$ can be developed as follows:

The jth moment of the population density is defined as

$$m_j(\Theta) = \int_0^\infty L^j n(\Theta,L)dL \tag{117}$$

Using equation(113), we get

$$m_j(\Theta) = \int_0^\infty dL \int_0^\infty L^j \bar{n}(\Theta,L;g^*)dg^* \tag{118}$$

Taking time derivatives of equation(118) yields

$$\frac{dm_j(\Theta)}{d\Theta} = \int_0^\infty dL \int_0^\infty L^j \frac{\partial \bar{n}(\Theta,L;g^*)}{\partial \Theta} dg^* \tag{119}$$

With the population balance equation (equation 116) this equation becomes

$$\frac{dm_j(\Theta)}{d\Theta} = -\int_0^\infty dL \int_0^\infty L^j g^* \frac{\partial \bar{n}(\Theta,L;g^*)}{\partial L} dg^* \tag{120}$$

and integrating by part yields

$$\frac{dm_j(\Theta)}{d\Theta} = j\int_0^\infty dL \int_0^\infty L^{j-1} g^* \bar{n}(\Theta,L;g^*)\, dg^* \tag{121}$$

The numerical solution of population balance equation (equation 116) by the method of characteristics reveals that the crystal population density, $\bar{n}(\Theta,L;g^*)$ is constant along characteristic lines of slope g^* in the Θ–L plane. The crystal population density of each subpopulation simply translates along the axis L unchanged in shape or proportion. After a certain increment of transformed time Θ all the crystals with growth rate activity g^* will have experienced an increase in size equal to the product of g^* and the increment in transformed time, Θ. Let λ be equal to the initial value of L at time zero such that $\bar{n}(\Theta,L;g^*) = \bar{n}(\lambda;g^*)$. At any time the size $L = \lambda + g^*\Theta$. Using this in equation (121) we get,

$$\frac{dm_j(\Theta)}{d\Theta} = j\int_0^\infty d\lambda \int_0^\infty g^*(\lambda+g^*\Theta)^{j-1} \bar{n}(\lambda;g^*)dg^* \tag{122}$$

As g* is determined randomly when a crystal is nucleated or introduced as a seed then the following expression holds

$$\bar{n}(\lambda;g^*) = P(g^*)n(\lambda) \tag{123}$$

Substituting this expression into equation (122) yields

$$\frac{dm_j(\Theta)}{d\Theta} = j\int_0^\infty (\lambda+g^*\Theta)^{j-1}n(\lambda)d\lambda \int_0^\infty g^*P(g^*)dg^* \tag{124}$$

From equation (124) the moments of the unknown growth rate activity distribution, P(g*), can be determined directly from the experimentally measured crystal size distributions.

From equation (124) for j = 1

$$\frac{dm_1(\Theta)}{d\Theta} = m_0\langle P(g^*)\rangle_1 \tag{125}$$

Integrating both sides with respect to Θ yields

$$\frac{m_1(\Theta)}{m_0} - \frac{m_1(0)}{m_0} = \Theta\langle P(g^*)\rangle_1 \tag{126}$$

For j = 2 after rearranging equation (124) we get

$$\begin{aligned}\frac{dm_2(\Theta)}{d\Theta} &= 2\int_0^\infty \lambda n(\lambda)d\lambda\int_0^\infty g^*P(g^*)dg^* + 2\Theta\int_0^\infty n(\lambda)d\lambda\int_0^\infty g^{*2}P(g^*)dg^* \\ &= 2[m_1(0)\langle P(g^*)\rangle_1 + \Theta m_0\langle P(g^*)\rangle_2]\end{aligned} \tag{127}$$

Integrating equation (127) with respect to Θ yields

$$\frac{m_2(\Theta)}{m_0} - \frac{m_2(0)}{m_0} = 2\Theta\frac{m_1(0)}{m_0}\langle P(g^*)\rangle_1 + \Theta^2\langle P(g^*)\rangle_2 \tag{128}$$

For j = 3

$$\frac{dm_3(\Theta)}{d\Theta} = 3\int_0^\infty \lambda^2 n(\lambda)d\lambda\int_0^\infty g^*P(g^*)dg^*$$

Table 11: Moments of growth rate activity distributions for anhydrous sodium sulphate crystals (Klug and Pigford[22])

seeded			Unseeded		
$\langle P(g^*)\rangle_1$ $\mu m/min$	$\langle P(g^*)\rangle_2$ $(\mu m/min)^2$	$\langle P(g^*)\rangle_3$ $(\mu m/min)^3$	$\langle P(g^*)\rangle_1$ $\mu m/min$	$\langle P(g^*)\rangle_2$ $(\mu m/min)^2$	$\langle P(g^*)\rangle_3$ $(\mu m/min)^3$
20	430	10 000	4.7	27	210
22	540	15 000	6.8	82	510
19	430	10 000	7.1	59	570

$$+ 6\Theta\int_0^\infty \lambda n(\lambda)d\lambda\int_0^\infty g^{*2}P(g^*)dg^*$$
$$+ 3\Theta^2\int_0^\infty n(\lambda)d\lambda\int_0^\infty g^{*3}P(g^*)dg$$
$$= 3m_2\langle P(g^*)\rangle_1 + 6\Theta m_1\langle P(g^*)\rangle_2 + 3\Theta^2 m_0\langle P(g^*)\rangle_3 \quad (129)$$

Integrating equation (129)

$$\frac{m_3(\Theta)}{m_0} - \frac{m_3(0)}{m_0} = 3\Theta\frac{m_2(0)}{m_0}\langle P(g^*)\rangle_1 + 3\Theta^2\frac{m_1(0)}{m_0}\langle P(g^*)\rangle_2 + \Theta^3\langle P(g^*)\rangle_3 \quad (130)$$

The three algebraic equations (equations 126, 128 and 130) can be solved to determine the first three moments of the growth rate activity distribution from the moments of the experimentally measured size distribution.

Typical results obtained from the measured size distribution from a batch crystallization of anhydrous sodium sulphate crystals with and without seeding as evaluated by graphical solution of algebraic equations (equations 126, 128 and 130) are reported in Table 11. All the moments for the growth rate activity distributions for this system have higher values in the case with seeding than those for the case without seeding. Thus experiments with the batch crystallizer showed that seed crystals added to the crystallizer grew with less growth dispersion and higher average growth rates than did the crystals

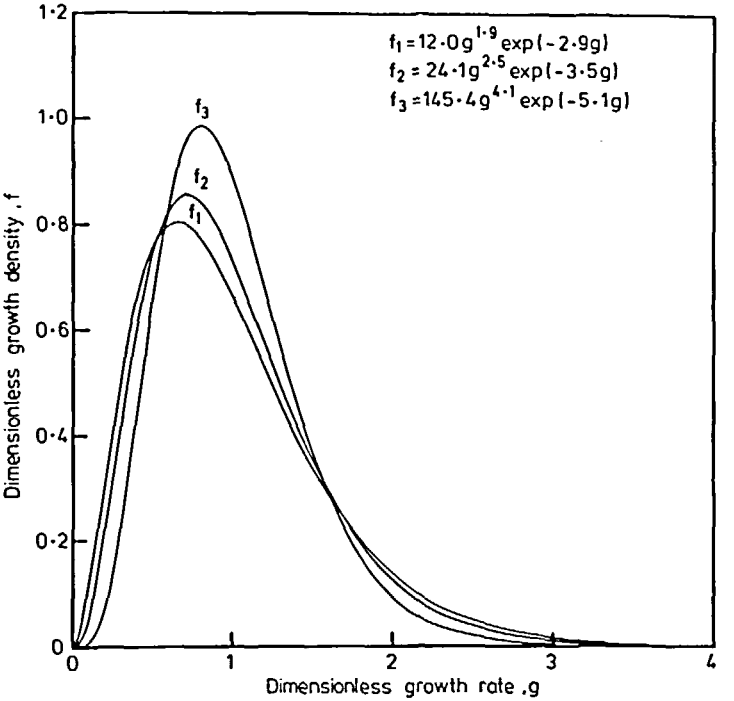

Figure 19 Normalized growth rate distribution at three levels of undercoolings

nucleated in the crystallizer. It was speculated that surface roughness of the seed crystals produced during their preparation and screening was responsible for this effect. Bohlin and Rasmuson[128] reported simulation studies of growth rate dispersion phenomenon in a cooling batch crystallizer accounting for primary, magma density dependent secondary nucleation and growth rate dispersion with constant crystal growth rate at different growth rate activities. The effect of growth rate dispersion and the shape of the growth rate activity distribution on the crystal size distribution was significant under certain conditions.

Berglund and Larson[129] reported a study of contact nucleation of citric acid monohydrate in a contact nucleation cell, the growth rate distributions being

formulated in the form of a gamma distribution. Figure 19 presents normalized growth rate distributions at three levels of undercoolings (1, 2 and 3 K at 303K, Table 3 of Berglund and Larson[129]), the value of the suffix representing their respective undercooling. These expressions can be used in deriving the normalized batch population density function for product crystals.

7. EVALUATION OF AGGLOMERATION KINETICS

Although the presence of agglomerates is fairly common the phenomenon of particle agglomeration and its characterization in such systems are not well understood. A number of recent studies[130-152](and see also Table 4 in Tavare[153]) provide illustrations of either numerical simulation techniques or characterization of kinetic rates in continuous, semi–batch and/or batch laboratory scale process units. The formation of agglomerated precipitates is usually linked with solution phase physicochemical and hydrodynamic interactions and the kinetic events are influenced by the environmental conditions. An understanding of the nature and extent of the effects of process parameters on the precipitation kinetic events may have implications for the development of design and operation guidelines. In this review the characterization of agglomeration kinetics will be illustrated with silica precipitation performed in a semi–batch crystallizer[152] as the results will be applicable directly to a batch reactive precipitation system. Furthermore reactive precipitation can be a useful paradigm for other agglomerating precipitates in food and pharmaceutical processes.

7.1 Reactive Precipitation

The manufacture of precipitated silica is essentially a neutralization process and can be represented by an overall reaction as

$$Na_2O\,(SiO_2)_x + H_2SO_4 \longrightarrow xSiO_2 \downarrow + Na_2SO_4 + H_2O \qquad (131)$$

It is usually carried out in two stages. The first stage, generally termed primary neutralization, constitutes a sol formation under alkaline conditions, in which the two reactants are added to a pool of water in such proportions that the pH of the system (or the degree of neutralization) is maintained at a constant value. The second stage, the secondary neutralization, involves addition of further acid in order to achieve complete neutralization. The sol is generally aged for some time prior to the second acid addition. Thus the overall process involves a discontinuous semi–batch operation.

Both solution chemistry during neutralization of silicate solution with acid and subsequent precipitation of silica are quite complex. Generally polymerization, i.e. the reactions that result in an increase in molecular weight of silica under a variety of process conditions, involves the condensation of silanol groups to give molecularly coherent units of increasing size either of spherical particles of increasing diameter or aggregates of an increasing number of constituent particles. Several analytical and empirical approaches based on polymerization studies have been suggested![54] The present study is concerned with the production of precipitated silica using mainly the industrial recipes and follow a process route under restricted operating conditions. The neutralization reaction between sodium silicate (alkali, B) and sulphuric acid (acid, A) for this manufacturing process may be considered as an elementary homogeneous archetype reaction

$$A + B \longrightarrow \text{products} \tag{132}$$

and the rate of disappearance of A or B by reaction may then be represented as

$$r_A = r_B = k_r c_A c_B \tag{133}$$

This representation of polymerization reactions by homogeneous reaction under restricted conditions and recipes may be reasonable. Under these experimental conditions almost all the product silica is in precipitated form rather than in gel form. A variety of techniques based on an empirical curve

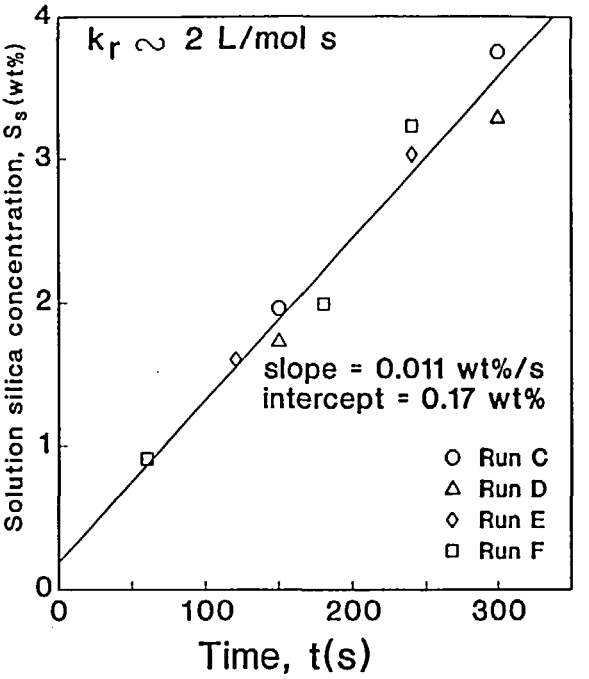

Figure 20 Initial silica concentration profile: reaction kinetics

fitting procedure have been suggested to characterize a rate equation![155] In the present case the rate constant in equation (133) can be evaluated by the method of initial rates determined from the concentration profiles of the solution silica in an initial period of the run where only neutralization occurs with negligible subsequent precipitation. Figure 20 shows an enlarged section depicting the solution silica concentration during the initial period of experimental runs. This concentration profile for initial period yields an approximate value of rate constant in equation 133 around 2.0 L/mol s. The reaction rate constant appears less than that for acid–alkali neutralization. This low value of the apparent reaction rate constant is probably due to complex physicochemical processes occurring in the liquid phase.

7.2 Population Balance

Precipitation processes often result in an agglomerated product. Agglomeration processes can be represented in the population balance by birth and death functions formulated on the basis of an empirical description and ensuing that they are written to ensure the principle of internal consistency. Although the precise mechanisms of agglomeration processes are difficult to model conceivably a simple mechanism based on two body collisions has generally been used in formulating the rate models (see for example Table 4, Tavare[153]). The agglomeration model proposed by Liao and Hulburt[156] used characteristic length as an additive property and provided analytical solutions for a continuous MSMPR crystallizer (see also Tavare et al[157]). Hartel and Randolph[130] presented their formulation in terms of crystal volume coordinates rather than the crystal size in order to incorporate aggregation and rupture terms in their numerical modelling of calcium oxalate aggregation behaviour. Hounslow et al[135] and Hounslow[140,141] in their numerical discretization scheme used a classical population balance approach in crystal size coordinates, transforming the conventional birth and death functions expressed in terms of crystal volume as the internal coordinate to the length based form. Tavare and Garside[152] in their study of silica precipitation in a semi–batch crystallizer used crystal volume coordinates.

For a perfectly mixed vessel the population balance equation in volume coordinates is

$$\frac{\partial \hat{n}_v}{\partial t} + G_v \frac{\partial \hat{n}_v}{\partial v} = \hat{B}_v - \hat{D}_v \tag{134}$$

where n_v is crystal population density function expressed as a function of crystal volume (no/m^3 kg) and G_v is the overall volume growth rate assumed for the sake of analytical simplicity to be crystal volume independent at least over small time interval. As the total working volume of the batch vessel is time varying the population density and other specific quantities, as used in crystal size domain, will be defined on the basis of total solvent capacity in

working vessel volume at any time and represented by a ^ over the corresponding symbol. For example volume population density $\hat{n}_v$ will be expressed as no/m^3. B_v and D_v represent the empirical birth and death functions over a volume between v and v + dv such that $(B_v - D_v)dv$ represents the net appearance of particles most probably by aggregation mechanism between v and v + dv. The aggregation of two particles of volume u and v − u into a particle volume v can be represented by the birth and death functions

$$\hat{B}_{va} = \frac{1}{2}\int_0^v \beta'(u,v-u)\hat{n}_v(t,u)\hat{n}_v(t,v-u)du \tag{135}$$

and

$$\hat{D}_{va} = \hat{n}_v(t,v)\int_0^\infty \beta'(u,v)\hat{n}_v(t,u)du \tag{136}$$

The agglomeration kernel $\beta(u,v-u)$ defined as

$$\beta(u,v-u) = \beta'(u,v-u)S \tag{137}$$

is a measure of the frequency of collisions between particles of particle volumes u and v–u that are successful in producing a particle of volume v. The factor $\frac{1}{2}$ in equation 8 ensures that collisions are not counted twice. The agglomeration kernel $\beta(u,v-u)$ depends on the environment surrounding the agglomerating crystal and accounts for the physical forces that are instrumental in the mechanism of aggregation, which decides its functional form. Although many theoretical and empirical formulations of the agglomeration kernel have been proposed to describe the various mechanisms of aggregation (see for example Drake[158], Hartel and Randolph[130], Hounslow et al.[135]) the agglomeration kernel is assumed to be crystal volume independent, at least over small time interval used for parameter identification of dynamic processes. When monodispersed spherical particles coagulate under the influence of Brownian motion the agglomeration can be independent of crystal volume. Both theoretical[130,135,158] and experimental[143,144,159] evidence suggests that the agglomeration kernel depends on crystal volume (or size).

For an unseeded batch crystallizer the pertinent boundary conditions to the population balance equation (equation 134) are

$$\hat{n}_v(0,v) = 0 \tag{138}$$

and

$$\hat{n}_v(t,0) = \hat{B}_{v0}/G_v \tag{139}$$

where B_{v0} is the nucleation rate of precipitate at near zero crystal volume. Equation 139 suggests that the particle flux of newly generated crystals added to the particulate system occurs at a vanishingly small volume very close to zero.

7.3 Moment Transformation

Following the treatment by Hulburt and Katz[80] the moment transformation of the population balance equation (equation 134) (in crystal volume coordinate) with respect to crystal volume, i.e., multiplying by v^j and integrating each term of equation 134 with respect to v over entire crystal volume range ($0 - \infty$), yields a set of ordinary differential equations in $\mu_{vj}(t)$ having the form

$$\frac{d\hat{\mu}_{vj}}{dt} = G_v[j\hat{\mu}_{vj-1} - \hat{n}_v v^j]_0^\infty] + \beta'\left[\frac{1}{2}\left[\sum_{k=0}^{j}\binom{j}{k}\hat{\mu}_{vk}\hat{\mu}_{vj-k}\right] - \hat{\mu}_{v0}\hat{\mu}_{vj}\right] \qquad j = 0,1,2,... \tag{140}$$

where $\binom{j}{k}$ is the binomial coefficient given by

$$\binom{j}{k} = \frac{j!}{k!(j-k)!} \tag{141}$$

Moment equations for the first three moments (up to second order) from equation 140 are

$$\frac{d\hat{\mu}_{v0}}{dt} = \hat{B}_{v0} - \tfrac{1}{2}\beta'\hat{\mu}_{v0}^2 \tag{142}$$

$$\frac{d\hat{\mu}_{v1}}{dt} = G_v\hat{\mu}_{v0} \tag{143}$$

$$\frac{d\hat{\mu}_{v2}}{dt} = 2G_v\hat{\mu}_{v1} + \beta'\hat{\mu}_{v1}^2 \tag{144}$$

with boundary conditions

$$\hat{\mu}_{vj} = 0 \qquad \text{at } t = 0 \qquad j = 0,1,2 \tag{145}$$

The population balance equation (equation 134) coupled with the moment equations (equations 142–144) together with appropriate boundary conditions represent the sufficient information about the batch reactive precipitation process that is required in parameter identification of particulate system in a reactive precipitation process.

7.4 Crystallization and Agglomeration Kinetics

The rate processes required to characterize an agglomerating reactive precipitation process are crystal growth, nucleation and agglomeration which can all be characterized by the method of moments analysis. In order to characterize the apparent rates associated with the evolution of the particulate system during the precipitation process several other techniques have been reported previously can easily be extended to the process representation. The experimentally determined population data can be converted into the moments with respect to crystal volume using the definition of moments

$$\hat{\mu}_{vj} = \int_0^\infty \hat{n}_v(t,v)v^j dv \tag{146}$$

These moments of the experimentally measured population density data can be used to determine the rates

$$G_v = \frac{\Delta\hat{\mu}_{v1}}{\hat{\mu}_{v0}\Delta t} \tag{147}$$

$$\beta' = \frac{\Delta\hat{\mu}_{v2}}{\bar{\hat{\mu}}_{v1}^{2}\,\Delta t} - \frac{2\,G_v}{\bar{\hat{\mu}}_{v1}} \tag{148}$$

and

$$\hat{B}_{v0} = \frac{\Delta\hat{\mu}_{v0}}{\Delta t} + \tfrac{1}{2}\beta'\bar{\hat{\mu}}_{v0}^{2} \tag{149}$$

where Δ represents the difference in values of the corresponding quantity at two different times and the overbar indicates an arithmetic average quantity. These three relations are derived from the moment equations (equations 142–144) by converting the derivatives in the differential equations into differentials. The average rates may be determined from the moments of two sets of experimental population density data obtained during the course of a batch experiment at times t and $t + \Delta t$.

Size distribution data obtained from the Coulter Counter measurements were translated into volume population density to calculate the growth, apparent nucleation and agglomeration rates via the method of moments analysis as described above. A typical pair of population density plots and its corresponding translation into volume population density curves are shown in Figure 21. In general the other results for both specific (expressed as no/m L or no/m^3 L) and total (expressed as no/m or no/m^3) population density (based on either size or volume) show the expected movement of the distribution with time, predominantly so during the sol formation step. Normally the spread in volume population density appears relatively more than that in size population density.

In order to estimate the rates using equations 147–149 the moments of observed population density were evaluated numerically from equation 146 by replacing the integral sign with summation. For all the runs results of successful evaluations of growth, nucleation and agglomeration rates using the method of moments analysis applied to successive population density curves (and also alternate successive runs in the case of runs where several samples with short time intervals were taken) can be evaluated along with other parameters required in kinetic correlations. All the results obtained may be

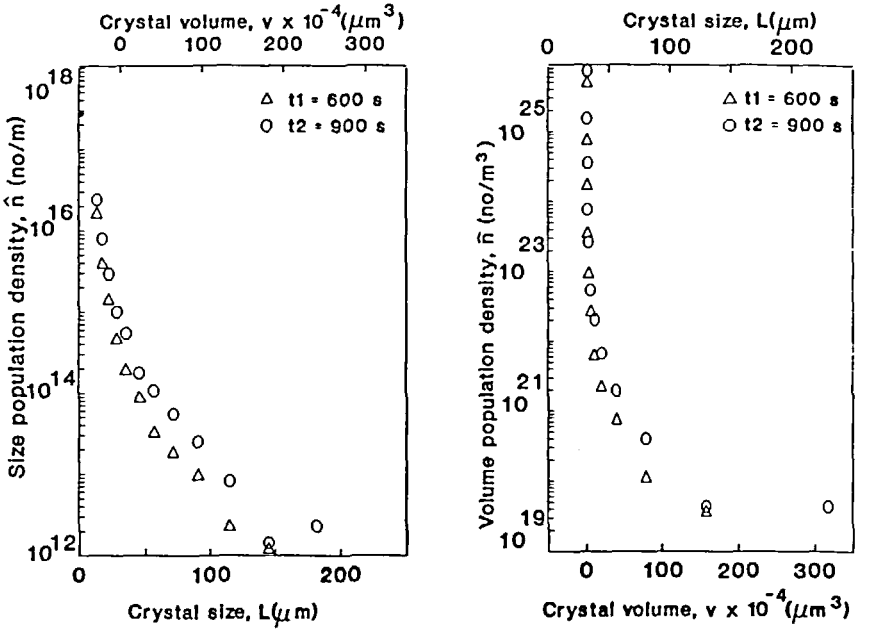

Figure 21 Population density plots in size and volume coordinates

correlated by empirical power law kinetic expressions in terms of *observables* as in many cases it is difficult to determine precisely conventional correlating variables like supersaturation and magma concentration during the experimental programme.

The present results of volumetric growth rates appeared consistent with the previously reported values of size growth rates as the previous average size growth rate is ~ 0.5×10^{-8} m/s[160] and its equivalent volumetric growth rate will be ~ 2×10^{-17} m^3/s. Perhaps both temperature and hydrodynamic conditions may influence growth kinetics. The calculated diffusional mass transfer coefficients for the present case using the literature correlations[161] was ~ 5×10^{-5} m/s and at 1 wt/wt % driving force the diffusional mass transfer rates were ~ 5×10^{-7} m/s early in the process indicating the diffusional process might

not be important in the primary neutralization stage. During ageing and secondary neutralization stages the overall process appeared to follow the equilibrium concentration profile suggesting that the surface processes were important.

The formation and behaviour of silica precipitates appear to depend on both chemical and environmental conditions. During the primary neutralization process i.e. the sol formation stage it is believed that primary particles are produced. These primary particles during their growth collide with each other to form secondary aggregates. In various coagulation or flocculating systems short range attractive forces are responsible for initially holding two particles together. These attractive forces may be homopolar, metallic, ionic or van der Waals forces and become important for submicron particle size. During the ageing process the suspension is allowed to stabilize within itself by growth, aggregation and break–up. In the secondary neutralization stage additional silica produced is deposited on the existing surface allowing the particles to form reorganized aggregates. Only small amount of silica is produced in the secondary neutralization stage resulting in small changes in particle size or volume distributions.

8 SUMMARY

In this review paper our understanding of the basic methods used in determining crystallization kinetics and characterizing the phenomenon of the growth rate dispersion has been summarized. This review is by no means a comprehensive work but it does give an idea of diversity of techniques that have been reported in the literature and illustrated in this review by numerical examples. Every process design of a batch crystallizer should be based on specific small scale tests with the liquors encountered and perhaps with the final tests in the apparatus under the conditions that actually simulate large scale equipment being considered or even in the plant equipment. Some of the techniques reported in this review can directly be considered for the actual industrial plant. Product specifications, system characteristics, economic

considerations and special problems pertaining to the system are important in batch crystallizer design and performance assessment. This review should serve as a starting point for the rational design, understanding and better utilization of batch crystallizers.

9 NOMENCLATURE

a	coefficient in growth rate correlation, constant
a'	empirical constant
a_i	coefficients in polynomial
A_T	total crystal surface area, m^2/kg solvent
AR	amplitude ratio
b	nucleation order
b	true estimates of β
b'	empirical constant
B	nucleation rate, no/kg solvent s
B_S	nucleation rate, kg solute/ kg solvent s
B_v	birth rate function, no/m^3 L s
B_{va}	birth rate function due to aggregation, no/m^3 L s
B_{v0}	nucleation rate, no/L s
BB	step length bound
c	concentration of solute, kg solute (or hydrate)/kg solvent, mol/L, wt%
c'	empirical constant, preexponential factor, kg solute/kg solvent
C_i	cosine Fourier transform of population density function at size L_i
CV	coefficient of variation, %
Δc	concentration driving force, kg solute (or hydrate)/kg solvent
D_G	effective growth rate diffusivity, m^2/s
D_v	death rate function, no/m^3 L s
D_{va}	death rate function due to aggregation, no/m^3 L s
D	diagonal scaling matrix
e	exponent of the ratio of slurry voidage to solid voidage

E_g	activation energy of growth process, kJ/mol
e_j	jth coordinate direction
f	dimensionless growth rate, $G/\bar{G}$
f(L)	seed CSD as a function of size
F	transfer function in Laplace transform and frequency domain
	ratio of surface to volume shape factor
$F(\beta)$	objective function used for optimization
g	growth rate order, dimensionless growth rate, $G/\bar{G}$
g^*	growth rate activity, μm/s
$\bar{g}^*$	average growth rate activity, μm/s
G	overall linear growth rate, m/s
G_v	overall crystal volume growth rate, m^3/s
ΔH	heat of crystallization, kJ/mol
i	relative kinetic order
I	impurity concentration, kg/kg
I	identity matrix
j	exponent of magma density, imaginary coefficient
J	Jacobian matrix
J^T	transpose of J
k	coefficient of impurity concentration, kg/kg
k_a	surface shape factor
k_b	nucleation rate constant, no/[kg s $(kg/kg)^{b+j}$]
k_B	nucleation rate constant, kg/[kg s $(kg/kg)^{b+j}$]
k_d	diffusional mass transfer coefficient, kg/[m^2s(kg/kg)]
k_g	overall linear growth rate constant, m/[s(kg/kg)g]
k_G	growth rate constant, kg/[m^2s$(kg/kg)^{-g}$]
k_v	volume shape factor
K	skewness
K_R	relative nucleation coefficient, no/[kg s $(m/s)^i(kg/kg)^j$]
L	crystal size, m,μm
LT	Laplace transform of
$L_{2,1}$	length weighted average size, m,μm
L	difference between successive sieve or channel size, m,μm
m	exponent of stirrer speed, number of observations

m_j	jth non–central moment of population density with respect to size, no m^j/kg solvent
M_T	suspension density, kg crystal/kg solvent
$M^{n,p}$	nth weighted moment at p in Laplace domain with respect to time
n	population density, no/m kg solvent
n^0	nuclei population density at zero size, no/m kg solvent
n_v	crystal volume population density, no/m^3 L
n(t,L)	population density function at size, L and time t, no/m kg solvent
$\bar{n}(t,L;g^*)$	population density of subpopulation with growth rate activity, g^* at size L
$\bar{n}(p,L)$	Laplace transform of response population density with respect to time
$\bar{n}(i\omega,L)$	Fourier transform of response population density with respect to time
$\lvert\bar{n}(i\omega,L)\rvert$	modulus representation of $\bar{n}(i\omega,L)$ i.e. magnitude ratio
$\angle\bar{n}(i\omega,L)$	argument representation of $\bar{n}(i\omega,L)$ i.e. phase shift
$\bar{n}(t,s)$	Laplace transform of response population density with respect to size
$\bar{n}(t,i\omega)$	Fourier transform of response population density with respect to size
$\lvert\bar{n}(t,i\omega)\rvert$	modulus representation of $\bar{n}(t,i\omega)$ i.e. magnitude ratio
$\angle\bar{n}(t,i\omega)$	argument representation of $\bar{n}(t,i\omega)$ i.e. phase shift
N	number of crystals, no/kg solvent; stirrer speed, rev/s
ΔN	number of crystals retained over ΔL; difference in cumulative number over ΔL
O( )	order of magnitude
p	Laplace variable with respect to time, 1/s
P(g^*)	growth rate activity distribution
$<P(g^*)>_j$	jth moment of growth rate activity distribution,$(\mu m/s)^j$
PS	absolute phase shift
p	direction of search vector
q	function $\{=\sqrt{[1+(4D_G p/\bar{G}^2)]}\}$

r	correlation coefficient; reaction rate, kmol/kg s, mol/L s
R	overall growth rate, kg/m^{2}s
R_g	gas constant, kJ/kmol K
s	Laplace transform variable with respect to size, 1/m
S	solvent capacity, kg
SD	standard deviation
S_i	sine Fourier transform of response population density
STEPMX	an estimate of the Euclidean distance
t	time, s
T	temperature, K,° C; dimensionless time (=t/τ)
u	dummy variable for crystal volume, m^3
v	crystal volume, m^3, μm^3
U_i	ith derivative of logarithmic transfer function
U_k	moment of dimensionless population density with respect to dimensionless time
V	volume of suspension, m^3, L
w	weight percent
W	mass of seed crystals, kg, kg/kg solvent
ΔW	weight of crystals retained on a sieve, kg
x	dimensionless crystal size, L/$\bar{G}\tau$
y	dimensionless population density, n/n^0; variable
Y	observable dependent variable, i.e. response (equation 36)

Greek Symbols

α	$3\rho_c/2F$, kg/m^3
α	step length
β	ratio of initial concentrations of reactants
β	agglomeration kernel, kg/no.s
β'	agglomeration kernel at any time for vessel volume, 1/no s
δ	delta dirac function
δ	correction or improvement vector
Δ	differential, difference
ϵ	solid voidage
ϵ	residual vector, i.e. difference between Y and η

μ	mean
μ_j	jth moment of population density with respect to time about the origin, no si^{*1}/m kg solvent
ν_j	jth central moment of population density, no mj/kg solvent
μ_{vj}	jth moment with respect to crystal volume, no m^{3j}/kg
ρ	density, kg/L
ρ_P	density of precipitated silica, kg/L
η	expected value of Y at x for given β
Δ	difference, differential
ρ_c	density of crystal, kg/m^3
$\phi(\sigma,T)$	dimensionless supersaturation function in the growth rate model
σ	supersaturation ratio $=(\frac{c-c^*}{c^*})$
σ^2	variance of impulse response
τ	run time, s
ω	frequency, 1/s, Fourier transform variables, 1/m, 1/s
λ	particle size at time $\Theta = 0$, μm; Marquardt parameter
Θ	new time variable, s
ζ_j	jth central moment of the growth rate activity

Subscript

A	acid
B	alkali, sodium silicate solution
b	bulk
E	end
f	final
L	at size L
N	newly generated, based on number
p	product, population
0	initial, feed, seed
p	precipitate
s	solution
sol	sol phase
soln	solution
S	silicate, seed, solute

t	total
1,2	addition stages
wm	weight mean

Superscript

–	average or transformed quantities
*	equilibrium, critical
.	derivative with respect to a variable
^	quantities based on total solvent capacity
0	nuclei

10. REFERENCES

1. Tavare, N. S., Chem. Eng. Commun., **61**, 259–318 (1987)
2. Ostwald, W., Zeitschrift für Physikalische Chemie, 22, 289–330 (1897)
3. Bisio, A. and R. L. Kabel, "*Scaleup of Chemical Processes*", John Wiley, New York (1985)
4. Kabel, R. L., Ind. Eng. Chem. Res., **31**, 641–643 (1992)
5. Larson, M. A., in "*Industrial Crystallization' 81*", S. J. Jancic and E. J. de Jong, ed, p 55–60, Budapest, Hungary (1981)
6. Garside, J. and R. J. Davey, Chem. Eng. Comun., 4, 393–424 (1980)
7. Garside, J., Chem Eng Sci, **40**, 3–26 (1985)
8. Randolph, A. D. and K. Rajagopal, Ind. Eng. Chem. Fundam., **9**, 165–171 (1970)
9. Randolph, A. D., Beckman J. R. and Z. I. Kraljevich, AIChE J, **23**, 500–509 (1977)
10. Shah, B. C., McCabe W. L. and R. W. Rousseau, AIChE J, **19**, 194 (1973)
11. Ness, J. N. and E. T. White, Chem. Eng. Prog. Symp. Ser. No. 72, **153**, 64–73 (1976)
12. Randolph, A. D. and S. K. Sikdar, AIChE J, 20, 410–412 (1974)

13. Evans, T. W., Margolis G. and A. F. Sarofim, AIChE J, 20, 959–966 (1974)
14. Palwe, B. G., Chivate M. R., and N. S. Tavare, Ind. Eng. Chem. Proc. Design Dev., 24, 914–919 (1985)
15. Jones, A. G. and J. W. Mullin, Chem. Eng. Sci., 29, 105–118 (1974)
16. Randolph, A. D. and M. A. Larson, "*Theory of Particulate Processes*", Acad. Press, New York (1971)
17. Tavare, N. S., Reviews in Chem. Eng., 7, 211–355 (1991)
18. Garside, J. and N. S. Tavare, Research Reports submitted to Separation Process Services (SPS), Harwell, Didcot (Oxn) (1982)
19. Garside, J. and N. S. Tavare, Chem. Eng. Res. Des., 64, 109–118 (1986)
20. Mullin, J. W. and J. Garside, Trans. I. Chem. E., 45, 285–290, 291–295 (1967)
21. Mullin, J. W. and J. Garside, Trans. I. Chem. E., 46, 11–18 (1968)
22. Klug, D. L. and R. L. Pigford, Ind. Eng. Chem. Res., 28, 1718–1725 (1989)
23. Tavare, N. S., Ind. Eng. Chem. Res., 30, 803–804 (1991b)
24. Prakash, R., Prakash O. and N. S. Tavare, Pramana –J Phys., 30, L597–L600 (1988)
25. Garside, J., Gibilaro L. G. and N. S. Tavare, Chem. Eng. Sci, 37, 1625–1628 (1982)
26. Tavare, N. S., AIChE J, 31, 1733–1735 (1985)
27. Misra, C. and E. T. White, Chem. Eng. Symp. Ser. 110, 67, 53–65 (1971)
28. Lyapunov, A. N. and E. P. Kholmogateseva, J. Appl. Chem. USSR, 30, 1379–1384, 1664–1668 (1957)
29. Mullin, J. W., Garside J. and C. Gaska, Chem. and Ind., 41, 1704–1706 (1966)
30. Nyvlt, J., J. Crystal Growth, 3/4, 377–383 (1968)
31. Janse, A. H. and E. J. de Jong, Trans. I. Chem. E., 56, 187 –193 (1978)
32. Hiquily, N. and C. Laguerie, in "*Industrial Crystallization'87*", (10th Symposium, Bechyne, Czechoslovakia) J. Nyvlt and S. Zacek, eds, Academia Prague and Elsevier, 107–110 (1989)

33. Toyokura, K., Yamazoe K., Magi J., Yago, N. and Y. Ayoma, in "*Industrial Crystallization*" , J. W. Mullin, Ed, Plenum Press, 41–52 (1976)
34. Toyokura, K., Uchiyama M., Kawai M., Akutsu H. and T. Ueno, in "*Industrial Crystallization*", S. J. Jancic and E. J. de Jong, Eds, North Holland Amsterdam, 87–96 (1982)
35. Garside, J. and M. B. Shah, Ind. Eng. Chem. Proc. Des. Develop., 19, 509–514 (1980)
36. Han, C. D., Chem. Eng. Sci., 22, 611–618 (1967)
37. Timm, D. C. and M. A. Larson, AIChE J, 14, 452–457 (1968)
38. Randolph, A. D. and M. D. Cise, AIChE J, 18, 798–806 (1972)
39. Youngquist, G. R. and A. D. Randolph, AIChE J, 18, 421–429 (1972)
40. Randolph, A. D. and S. K. Sikdar, Ind. Eng. Chem. Fundam., 15, 64–71 (1976)
41. Sowul, L. and M. A. F. Epstein, AIChE Symp Ser. 193, 71, 73–81 (1980)
42. Dauday, P. J. and E. J. de Jong, in "*Industrial Crystallization 84*", S. J. Jancic and E. J. de Jong, Eds, Elsevier, Amsterdam, 447–451 (1984)
43. Tavare, N. S., Can. J. Chem. Eng., 64, 752–758 (1986)
44. Omran, A. M. and C. J. King, AIChE J, 20, 795–802 (1974)
45. Kane, S. G., Evans T. W., Brian P. L. and A. F. Sarofim, AIChE J, 20, 855–862 (1974)
46. Stocking, J. H. and C. J. King, AIChE J, 22, 131–140 (1976)
47. Shirai, Y., Nakanishi K., Matsuno, R. and T. Kamikubo, AIChE J, 31, 676–682 (1985)
48. Shi, Y., Liang, B. and R. W. Hartel, in "*Crystallization as a Separation Process*", A. S. Myerson and K. Toyokura, ed., ACS Symp. Ser. No. 438, 316–328, ACS Washington DC (1990)
49. Kyprianidou–Leodidou, T. C. and G. D. Botsaris, in "*Crystallization as a Separation Process*", A. S. Myerson and K. Toyokura, eds, ACS Symp. Ser. No 438, 364–372, ACS, Washington DC (1990)
50. Halfon, A. and S. Kaliguine, Can. J. Chem. Eng., 54, 160–167 (1976)
51. Verigin, A. N., Shuhuplyak, I. A., Mikhalev M. F. and V. N. Kulikov, J. Appl. Chem. USSR, 52, 1801–1803 (1980)

52. Marquardt, D. W., J. Soc. Ind. Appl. Math, 11, 431–441 (1963)
53. Powell, M. J. D., Computer J., 8, 303–307 (1965)
54. Bellman, R., and R. Kalaba, "*Quasilinearization and Non–linear Boundary Value Problems*", American Elsevier, New York (1965)
55. Lee, E. S., "*Quasilinearization and Invarient Imbedding*", Academic Press, New York (1968)
56. Seinfeld, J. H. and G. R. Gavalas, AIChE J, 16, 644–647 (1970)
57. Seinfeld, J. H. and L. Lapidus, "*Mathematical Methods in Chemical Engineering*", Prentice Hall, Englewood Cliffs, New York (1974)
58. Donnelly, J. K. and D. Quon, Can. J. Chem. Eng., 48, 114 –119 (1970)
59. Nieman, R. E. and D. G. Fisher, Can. J Chem. Eng., 50, 802–806 (1972)
60. Wang, B.C. and Luss R., Int. J. Control, 31, 947–972 (1980)
61. Hwang, M. and J. H. Seinfeld, AIChE J, 18, 90–93 (1972)
62. Bergmann, R. N., Kalaba R. E. and K. Spingarn, J Optimization Theory Applications, 20, 47–63 (1976)
63. Xugen, V. T. and W. Y. Svrcek, J Optimization Theory Applic., 22, 117–123 (1977)
64. Kalogerakis, N. and R. Luss, AIChE J, 29, 858–866 (1983)
65. Qiu, Y. and A. C. Rasmuson, AIChE J, 36, 665–676 (1990)
66. Qiu, Y. and A. C. Rasmuson, Chem. Eng. Sci. 46, 1659–1667 (1990)
67. Witkowski, W. R., S. M. Miller and J. B. Rawlings, in "*Crystallization as a Separation Process*", A. S. Myerson and K. Toyokura, ed., ACS Symp. Ser. No. 438, 102–114, ACS Washington DC (1990)
68. Rawlings, J. B., Miller S. M. and W. R. Witkowski, Ind. Eng. Chem. Res., 32, 1275–1296 (1993)
69. Bransom, S. H. and W. J. Dunning, Discuss Faraday Soc., 5, 96–111 (1949)
70. Wey, J. S. and J. Estrin, Ind. Eng. Chem. Process Des. Develop., 12, 236–246 (1973)
71. Estrin, J., McNeil T. J. and D. R. Weed, AIChE J, 24, 728–731 (1978)
72. Lee, H. H., AIChE J., 24, 535–537 (1978)
73. Wey, J. S. and J. P. Terwilliger, AIChE J, 25, 208 (1979)
74. Harano, Y. and H. Yamamoto, J. Chem. Eng. Japan, 13, 313–318 (1980)

75. Harano, Y. and H. Yamamoto, in "*Industrial Crystallization 81*", S. J. Jancic and E. J. de Jong, eds, North Holland, Amsterdam, 137–145 (1982)
76. Gutwald, T. and A. Mersmann, in "*Industrial Crystallization'90*", A. Mersmann, ed, p 331–336, Garmisch–Partenkirchen, Germany (1990)
77. Molner, I., Halas S. and T. Bickle, Chem. Eng. Sci., 45, 1243–1251 (1990)
78. Seinfeld, J. H., Chem. Eng. Sci., 24, 65–74 (1969)
79. Seinfeld, J. H. and W. H. Chan, Chem. Eng. Sci., 26, 753–766 (1971)
80. Hulburt, H. M. and S. Katz, Chem. Eng. Sci., 19, 555–574 (1964)
81. Janse, A. H., "*Nucleation and Crystal Growth in Batch Crystallizers*", Ph D Thesis, Delft University of Technology (1977)
82. Jancic, S. J., "*Crystallization Kinetics and Crystal Size Distribution in Mixed Suspension Mixed Product Removal Crystallizers*", Ph D Thesis, University College, London (1976)
83. Garside, J. and S. J. Jancic, AIChE J, 25, 948–958 (1979)
84. Mullin, J. W. and J. Nyvlt, Kristall und Technik, 9, 141–155 (1974)
85. Nyvlt, J.,"*Industrial Crystallization: The Present State of Art*", Verlag Chemie, Weinheim (1978)
86. White, E. T. and P. G. Wright, Chem. Eng. Prog. Symp. Ser. 110, 67, 81–87 (1971)
87. Natalina, L. N. and E. B. Treivus, Sov. Phys. Crystallogr., 19, 389–391 (1974)
88. Janse, A. H. and E. J. de Jong, in "*Industrial Crystallization 78*", S. J. Jancic and E. J. de Jong, eds, North Holland, Amsterdam, 135–142 (1979)
89. Gabas, N. and C. Laguerie, Chem. Eng. Sci., 46, 1411–1418 (1991)
90. Garside, J., in "*Industrial Crystallization'78*", S. J. Jancic and E. J. de Jong, Eds, North Holland Publishing Co., Amsterdam, 143–151 (1979)
91. Garside, J., Rusli I. T. and M. A. Larson, AIChE J, 25, 57–64 (1979)
92. Garside, J., Rusli I. T. and M. A. Larson, AIChE Symp. Ser. 193, 76, 52–58 (1980)
93. Berglund, K. A. and M. A. Larson, The second World Congress of Chemical Engineering, Montreal, Canada, 72–75 (1981)

94. Berglund, K. A., Kaufman E. L. and M. A. Larson, AIChE J, 29, 867–869 (1983)
95. Berglund, K. A. and M. A. Larson, AIChE Symp Ser 215, 78, 9–13 (1982)
96. Berglund, K. A. and J. J. Mathis–Lilley, AIChE J, 31, 865–867 (1985)
97. Berglund, K. A. and B. H. Shanks, AIChE J, 31, 152–154 (1985)
98. Bujac, P. D. B., in "*Industrial Crystallization*" (6th Symposium, Usti nad Labem), J. W. Mullin, Ed, Plenum Press, New York, 23–31 (1976)
99. Purves, W.T. and M. A. Larson, IChemE Symp. Ser. Solid Separation Processes No. 59, 7:5/1–18 (1980)
100. Ramanarayanan, K. A., Berglund K. A. and M. A. Larson, Chem. Eng. Sci., 40, 1604–1608 (1985)
101. Girolami, M. W. and R. W. Rousseau, Ind. Eng. Chem. Process Des. Dev., 25, 66–70 (1988)
102. Girolami, M. W. and R. W. Rousseau, AIChEJ, 31, 1821–1828 (1985)
103. Zumstein, R. C. and R. W. Rousseau, AIChE J., 33, 121–129 (1987)
104. Zumstein, R. C. and R. W. Rousseau, AIChE J, 33, 1921–1925 (1987)
105. Valcic, A. V., J. Crystal Growth, 30, 129–136 (1975)
106. Davey, R. J., Ristic R. I. and B. Zizic, J Crystal Growth, 47, 1–4 (1979)
107. Garside, J. and R. I. Ristic, J Crystal Growth, 61, 215–220 (1983)
108. Tavare, N. S. and J. Garside, in "*Industrial Crystallization 81*", S. J. Jancic and E. J. de Jong, Eds, North Holland, Amsterdam, 21–27 (1982)
109. Tavare, N. S. and J. Garside, Trans. Inst. Chem. Engrs., 60, 334–344 (1982)
110. Janse, A. H. and E. J. de Jong, in "*Industrial Crystallization*", J. W. Mullin, ed, Plenum Press, New York, 145–154 (1976)
111. Larson, M. A., White E. T., Ramnarayanan K. A and K. A. Berglund, paper presented at AIChE annual meeting, Los Angeles, CA (1982)
112. Randolph, A. D. and E. T. White, Chem. Eng. Sci., 32, 1067–1076 (1977)
113. Wen, C. Y. and L. T. Fan, "*Models For Flow Systems And Chemical Reactors*", Marcel Dekker, Inc., New York, 113–208 (1975)
114. Clements, Jr W. C., Chem. Eng. Sci., 24, 957–963 (1969)

115. Abbi, Y. P. and D. J. Gunn, Trans I Chem E, 54, 225–237 (1976)
116. Michelsen, M. L. and K. Ostergaard, Chem. Eng. Sci., 25, 583–592 (1970)
117. Williams, J. A., Alder R. J. and W. J. Zolner, Ind. Eng. Chem. Fundam., 9, 193–197 (1970)
118. Rosen, J. B. and W. E. Winsche, J. Chem. Phys., 18, 1587–1597 (1950)
119. Jeffreson, C. P., Chem. Eng. Sci., 25, 1319–1329 (1970)
120. Aris, R., Chem. Eng. Sci., 9, 266–267 (1959)
121. Garside, J. and S. J. Jancic, AIChE J, 22, 887–894 (1976)
122. Tavare, N. S. and J. Garside, Chem. Eng. J., 25, 229–232 (1982)
123. Aris, R., Proc Royal Soc., A235, 67–78 (1956)
124. Anderssen, A. S. and E. T. White, Chem. Eng. Sci., 26, 1203–1221 (1971)
125. Hopkins, M. J., Sheppard A. J., and P. Eisenklam, Chem. Eng. Sci., 24, 1131–1137 (1969)
126. Clements, Jr W. C. and K. B. Jr. Schenelle, Ind. Eng. Chem. Process Des. Dev., 2, 94–102 (1963)
127. Johnson, J. L., Fan L. T. and Y. S. Wu, Ind. Eng. Chem. Process Des. Dev., 10, 425–431 (1971)
128. Bohlim, M. and A. C. Rasmuson, AIChE J, 38, 1853–1863 (1992)
129. Berglund, K. A. and M. A. Larson, AIChE J, 30, 280–287 (1984)
130. Hartel, R. W. and A. D. Randolph, AIChE J., 32(7), 1186–1195 (1986)
131. Hartel, R. W., Gottung B. E., Randolph A. D. and G. W. Drach, AIChE J., 32(7), 1176–1185 (1986)
132. Delpech de Saint Guilhem, X., and T. A. Ring, Chem. Eng. Sci., 42, 1247–1249 (1987)
133. Lamey, M. D. and T. A. Ring, Chem. Eng. Sci, 41, 1213–1219 (1988)
134. Franck, R., David, R., Villermaux, J. A. and J. P. Klein, Chem. Eng. Sci., 43, 69–77 (1988)
135. Hounslow, M. J., Ryall R. L. and V. R. Marshall, AIChE J., 34(11), 1821–1832 (1988)
136. Marchal, P., David R., Klein, J. P. and J. Villermaux, Chem. Eng. Sci., 43, 59–67 (1988)
137. Sohnel, O., Mullin, J. W. and A. G. Jones, Ind. Eng. Chem. Res., 27, 1721–1728 (1988)

138. Przybycien, T. M., and J. E. Bailey, AIChE J., 35(11), 1779–1790 (1989)
139. Zumstein, R. C., and R. W. Rousseau, Chem. Eng. Sci., 44(10), 2149–2155 (1989)
140. Hounslow, M. J., AIChE J., 36(1), 106–116 (1990)
141. Hounslow, M. J., AIChE J., 36(11), 1748–1751 (1990)
142. Chen, W., R. R. Fisher and J. C. Berg, Chem. Eng. Sci., 45, 3003–3006 (1990)
143. David, R., Marchal P., Villermaux J. and J. P. Klein, Chem. Eng. Sci., 46, 205–213 (1991)
144. David, R., Villermaux J., Marchal P. and J. P. Klein, Chem. Eng. Sci., 46, 1129–1136 (1991)
145. Masy, J. C. and M. Cournil, Chem. Eng. Sci., 46, 693–701 (1991)
146. Hostomsky, J. and A. G. Jones, J. Phys. D: Applied Phys., 24, 165–170 (1991)
147. Dirksen, J. A. and T. A. Ring, Chem. Eng. Sci., 46, 2389–2427 (1991)
148. Tavare, N. S. and A. V. Patwardhan, AIChE J., 38, 377–384 (1992)
149. Wachi, S. and A. G. Jones, Chem. Eng. Sci., 47, 3145–3148 (1992)
150. Lui, R. Y. M. and R. W. Thompson, Chem. Eng. Sci., 47, 1897–1901 (1992)
151. Bhatia, S. K. and D. Chakraborty, AIChE J, 38, 868–878 (1992)
152. Tavare, N. S. and J. Garside, Chem. Eng. Sci, 48, 475–488 (1993)
153. Tavare, N. S., AIChE J, 32, 705–732 (1986)
154. Iler, R. K., "*Chemistry of Silica*", John Wiley, New York (1979)
155. Levenspiel, O., "*Chemical Reaction Engineering*", 2nd ed, John Wiley, New York (1972)
156. Liao, P. F. and H. M. Hulburt, "*Agglomeration Processes in Suspension Crystallization*", Annual Meeting of AIChE, Chicago, (Dec 1976)
157. Tavare, N. S., Shah M. B. and J. Garside, Powder Technology, 44, 13–18 (1985)
158. Drake, R. L., in "*Topics in Current Aerosol Research*", part 2, G. M. Hidy and J. R. Brock, eds, Pergaman Press, New York (1972)
159. Higashitani, K., Yamauchi K., Matsuno Y. and G. Hosokawa, J. Chem. Eng. Japan, 16(4), 299–304 (1983)

160. Tavare, N. S., and J. Garside, in "*Recent Trends in Chemical Reaction Engineering*", Vol II, p 272–280, B. D. Kulkarni, R. A. Mashelkar and M. M. Sharma, Eds, Wiley Estern, New Delhi (1987)
161. Nienow, A., Chem. Eng. J, 9, 153–161 (1975)
162. Mohamed–Kheir, A. K. M., Tavare N. S. and J. Garside, in "*Crystallization and Precipitation*", G. L. Strathdee, M. O. Klein, L. A. Melis, Eds, 61–70, Pergamon Press, Oxford (1987)